

# Flexible goal-oriented space-time adaptivity for coupled Stokes flow and convection-dominated transport

Markus Bause<sup>a</sup>, Marius Paul Bruchhäuser<sup>\*,a</sup>, Uwe Köcher<sup>a</sup>

<sup>a</sup>*Helmut Schmidt University, Faculty of Mechanical Engineering, Holstenhofweg 85, 22043 Hamburg  
bause@hsu-hh.de, bruchhaeuser@hsu-hh.de (\*corresponding author),  
koecher@hsu-hh.de.*

## Abstract

In this work, a flexible, fully space-time adaptive finite element approximation of a prototype multi-physics system coupling fluid flow and convection-dominated transport is developed and studied. By some minor generalization, the model becomes feasible for the simulation of a poroelasticity system. Automatic mesh adaptation is based on the Dual Weighted Residual method for goal-oriented a posteriori error estimation. In multi-physics, the reliable and economical computation of a specific functional, the so-called quantity of interest, is typically desirable. Here, adaptive algorithms become more involved since they need not only to control the time and space meshes, but also need to balance the contributions of the coupled subproblems to the error in the goal quantity. Key ingredients of the presented approach are the discontinuous Galerkin time discretization for the primal and dual problem of the DWR approach, permitting miscellaneous evaluations of the DWR error estimator, its implementation in an advanced software architecture and the separation of effects of temporal and spatial discretization which facilitates the simultaneous adjustment of the time and space mesh.

**Keywords:** Poroelasticity, coupled systems, space-time adaptivity, goal-oriented a posteriori error control, Dual Weighted Residual method

**2019 MSC:** 11–30, 01–25

## 1. Introduction

### 1.1. Poroelasticity

Recently, the quasi-static Biot system (cf., e.g., [25, 31]) has attracted researcher's interest and been studied for the numerical simulation of flow in deformable porous media. It models fluid-structure interaction by coupling fluid flow in a porous medium with the mechanical response and deformation of the medium. The quasi-static Biot system offers important applications in natural sciences and technology, including modern material science polymers and metal foams, gaining significance particularly in lightweight design and aircraft industry, design of batteries or hydrogen fuel cells for green technologies, filtering, geothermal energy exploration or reservoir engineering as well as mechanism in the human body (biomedicine) and food technology. The quasi-static Biot system reads as

$$-\nabla \cdot \boldsymbol{\sigma}(\mathbf{u}) + \alpha \nabla p = \mathbf{f}, \quad (1.1a)$$

$$\partial_t(\kappa_0 p + \alpha \nabla \cdot \mathbf{u}) + \nabla \cdot \mathbf{v}_f = \phi, \quad (1.1b)$$

to be solved in  $\Omega \times (0, T]$ , where  $\boldsymbol{\sigma}(\mathbf{u}) := \mu \boldsymbol{\varepsilon}(\mathbf{u}) + \lambda \nabla \cdot \mathbf{u} \mathbf{I}$ ,  $\boldsymbol{\varepsilon}(\mathbf{u}) := \frac{1}{2}(\nabla \mathbf{u} + \nabla \mathbf{u}^\top)$  and  $\mathbf{v}_f := \frac{\mathbf{K}}{\mu_f}(\nabla p - \rho_f \mathbf{g})$ . The set of equations (1.1) has to be closed by initial and boundary conditions. In (1.1), the unknown  $\mathbf{u}$  denotes the displacement field of the porous medium,  $\boldsymbol{\sigma}(\mathbf{u})$  the effective stress tensor with linearized strain tensor  $\boldsymbol{\varepsilon}(\mathbf{u})$  and Lamé parameters  $\mu$  and  $\lambda$ ,  $\mathbf{I}$  denotes the identity tensor and  $\mathbf{f}$  is a body force. Further,  $p$  is the fluid's pressure,  $\alpha$  is the Biot–Willis constant and  $\kappa_0$  is the specific storage coefficient. Finally, by  $\mathbf{v}_f$  we denote the Darcy velocity or fluid flux, by  $\mathbf{K}$  the permeability tensor, by  $\mu_f$  the fluid's viscosity and by  $\rho_f$  its density,  $\mathbf{g}$  is the gravity or, in general, some body force and  $\phi$  is a volumetric source.

It's well known that a vanishing storage coefficient (i.e. incompressible fluid)  $\kappa_0 = 0$  may exhibit a locking phenomenon in discretizations; cf., e.g., [24, 21] and the discussion therein. One remedy, that is introduced in [15], to overcome non-robustness of the discretization with respect to  $\kappa_0$  is to reformulate the Biot system (1.1) by introducing the additional (artificial) variables  $q := \nabla \cdot \mathbf{u}$ ,  $p := \kappa_0 p + \alpha q$  and  $\xi := \alpha p - \lambda q$ . Then, we recover

Biot's equations (1.1) as

$$-\mu \nabla \cdot \varepsilon(\mathbf{u}) + \nabla \xi = \mathbf{f}, \quad (1.2a)$$

$$k_3 \xi + \nabla \cdot \mathbf{u} = k_1 \eta, \quad (1.2b)$$

$$\partial_t \eta - \frac{1}{\mu_f} \nabla \cdot (\mathbf{K}(\nabla(k_1 \xi + k_2 \eta) - \rho_f \mathbf{g})) = \phi. \quad (1.2c)$$

It directly follows that

$$p = k_1 \xi + k_2 \eta \quad \text{and} \quad q = k_1 \eta - k_3 \xi,$$

where  $k_1 := \alpha/(\alpha^2 + \lambda \kappa_0)$ ,  $k_2 := \lambda/(\alpha^2 + \lambda \kappa_0)$  and  $k_3 := \kappa_0/(\alpha^2 + \lambda \kappa_0)$ . In (1.2), the generalized Stokes problem (1.2a), (1.2b) for the displacement field  $\mathbf{u}$  and the pseudo pressure variable  $\xi$  is coupled with the diffusive transport problem (1.2c) for the pseudo pressure variable  $\eta$ .

### 1.2. Model problem

In this work, we study goal-oriented space-time adaptivity for the finite element approximation of the coupled Stokes flow and transport system

$$-2\tilde{\nu} \Delta \mathbf{v} + \nabla p = \mathbf{f} \quad \text{in } \Omega, \quad (1.3a)$$

$$\nabla \cdot \mathbf{v} = 0 \quad \text{in } \Omega, \quad (1.3b)$$

equipped with appropriate boundary conditions, and

$$\rho \partial_t u - \nabla \cdot (\varepsilon \nabla u) + \mathbf{v} \cdot \nabla u + \alpha u = g \quad \text{in } Q = \Omega \times I, \quad (1.4a)$$

$$u = 0 \quad \text{on } \Sigma_D = \partial\Omega \times I, \quad (1.4b)$$

$$u = u_0 \quad \text{on } \Sigma_0 = \Omega \times \{0\}. \quad (1.4c)$$

The system (1.3), (1.4) is studied due to its prototype character for a wide range of applications in practice. The goal-oriented adaptivity approach that is developed in this work is general enough such that it can be adapted to multi-physics systems with a coupling structure similar to that of (1.3), (1.4). In particular, its adaptation to the poroelasticity model (1.2) is straightforward.

In (1.3), (1.4), we denote by  $\Omega \subset \mathbb{R}^d$ , with  $d = 2, 3$ , a polygonal or polyhedral bounded domain with Lipschitz boundary  $\partial\Omega$  and  $I = (0, T]$ ,  $0 < T < \infty$ , is a finite time interval. Further,  $\nu := 2\tilde{\nu}$  is the fluid's kinematic viscosity. We assume that  $\varepsilon > 0$  is a constant diffusion coefficient,  $\alpha \in L^\infty(\Omega)$  is the reaction coefficient,  $\rho > 0$  is the constant density coefficient. Homogeneous Dirichlet boundary conditions in the flow and transport problem are prescribed for brevity only. In our numerical examples in Sec. 5 we also consider more general boundary conditions. For the sake of physical realism, the transport problem is supposed to be convection-dominated by letting  $0 < \varepsilon \ll |\mathbf{v}(\mathbf{x})|$ . Well-posedness of (1.3), (1.4) and the existence of a sufficiently regular solution  $(\mathbf{v}, p, u)$ , such that all of the arguments and terms used below are well-defined, are tacitly assumed without mentioning explicitly all technical assumptions about the data and coefficients.

### 1.3. Previous work

Goal-oriented error control and its application for the adjustment of the computational mesh can be traced back to Becker and Rannacher [4]. In this approach the error in the approximation of certain quantities of physical interest is estimated in terms of local residuals of the computed solution multiplied by sensitivity factors that are obtained by solving the associated dual problem of the given equations. Therefore, it is referred to as the **D**ual **W**eighted **R**esidual method. Since the pioneering work in duality based error estimation, numerous studies have been done for the application of the DWR method to several classes of problems of physics including coupled phenomena and problems of optimal control. In particular, goal-oriented error control was strongly analyzed for the computation of nonstationary incompressible flow modeled by the Navier–Stokes equations. For this, we refer to, e.g., [6] and the references therein. Moreover, the economical simulation of fluid-structure interaction as a prominent system of multi-physics has attracted the usage of a posteriori error control mechanisms based on duality techniques. For this, we refer to, e.g., [27, p. 340]. Generalized versions of the DWR method in that not only the discretization error but also the iteration or a modelling error is addressed, have been developed and studied; cf., e.g., [26, 7]. Further generalizations consider multi-objective goal functionals or the treatment of higher-order corrections of the error estimator that are often neglected. Nevertheless, there is still an ongoing work in the design and further improvement of DWR based space-time adaptivity in the finite element method; cf., e.g., [12, 13] for recent work. In [12], error localization of the DWR method is performed in a variational form using a partition-of-unity approach, instead of evaluating strong operators (up to second order) and face integrals, as it is done in the classical way of error localization [4]. Thereby, node-wise error contributions

are obtained and computational costs are reduced. In particular, this advantage emerges in the DWR-based approximation of systems of partial differential equations [32]. For a further review of related techniques of weakly-based localization we refer to [12]. We note that for the DWR method no rigorous justification for convergence and optimality of the adaptive algorithm exists so far, but only excellent practical observations. Recently, efficiency and reliability results that are highly desirable in a posteriori error control were proved for a computable DWR estimator in [13]. This is done in an abstract Banach space setting under saturation assumptions about the goal functional. Further, hierarchical approximations of the primal and dual solution in enriched finite element spaces for evaluating the DWR error estimator, involving the primal and dual residual, are used. For general goal functionals the proof of the saturation assumptions that is widely used in hierarchical a posteriori error estimation continues to remain an open problem. In [13], bounds for effectivity indices are further established. Numerical experiments are presented for stationary problems. For further efficiency and reliability results we refer to the references given in [13]. In addition, we mention the discussion in the DWR literature (cf., e.g., [4, 9, 10, 13] and the references therein) regarding the usage of computationally expensive enriched finite element spaces versus (patch-wise) interpolation for the evaluation of the error estimator.

DWR based error control has been well understood for single-physics problems. Rigorous studies of DWR techniques for *nonstationary* multi-physics systems and their numerical validations are still rare in the literature. One reason for this might be that the separation of contributions to the discretization error and the control of the temporal and spatial mesh becomes more involved since, in addition, the impact of each of the subproblems and its approximation on the goal quantity has to be understood and balanced within the localized error representation and mesh refinement process. In [23], goal oriented adaptivity for a coupled Darcy flow and transport system is developed which is related to this work. In [23], a continuous piecewise linear approximation in space and time for the approximation of the transport equation is studied only. Further, in [23] adaptivity is considered only in space but not in time.

Finally, we note that the effectivity and efficiency of goal-oriented space-time adaptive methods demands on their efficient software implementation. This requires the appropriate selection and implementation, respectively, of data structures and efficient algorithms acting on them. Recently, a programming model for the DWR approach applied to the nonstationary diffusion equation with fixed lowest-order time discretizations for the primal and dual problem was published by the authors in [22].

In (1.4), convection-dominated transport is comprised by assuming that  $0 < \varepsilon \ll |\mathbf{v}(\mathbf{x})|$ . This puts an additional facet of complexity in the reliable and parameter robust numerical approximation of (1.4) and the a posteriori error control. For a survey of the current state of the research in the field of numerical approximation of convection-dominated problems we refer to [19]. The application of goal-oriented error control to nonstationary convection-dominated transport is reviewed and studied by two of the authors in [10]. Results of the literature for a posteriori error estimation of convection-dominated transport are referenced therein as well.

#### 1.4. New contributions

In this work, a coupled flow and transport prototype model is studied. Such systems arise in numerous applications of practical interest. Recently, the design of multirate schemes for such coupled problems have attracted researchers' interest; cf., e.g., [1, 14, 16]. In multirate approaches, the coupled subproblems are solved on different time meshes, even different spatial meshes for the subintervals may be encountered in the future, depending on the time scales of the solutions to the subproblems. Typically, the flow problem, being computationally more expensive, is solved on a coarser time mesh than the transport problem of higher dynamics. To the best of our knowledge, the DWR method has not been studied yet for multirate approximations of multi-physics. Multirate techniques require a revision and more careful application of the DWR method compared to the singlerate framework studied so far. A first step in this direction is performed here. This work is characterised by the following features in the application of the DWR method. Thereby it differs in parts from previous works. The flexibility offered here will allow the development of multirate DWR approaches in a future work.

- An arbitrary order discontinuous Galerkin (dG) time discretization is rigorously applied to the primal and dual problem. This frees us from the application of higher-order interpolation or combinations of discontinuous with continuous Galerkin time discretizations for the evaluation of the DWR error estimator; cf., e.g., [3, 6, 10, 30]. We recall that in the DWR method the respective *weights* cannot be solved in the same finite element space since otherwise the whole error identity would vanish; cf., e.g., [4, Ch. 4.1] and Sec. 4 in this work. In [10], the implicit Euler method that can be recovered as discontinuous piecewise constant Galerkin approximation in time and the Crank–Nicholson scheme that can be interpreted as a continuous piecewise linear approximation in time are used for the time integration of the primal and dual problem, respectively. In [3, 6, 30] higher-order interpolation is applied. We note that the discontinuous Galerkin method, applied to ordinary differential equations, is known to be strongly *A*-stable (or *L*-stable, respectively), which is considered to be advantageous for stiff systems, whereas the continuous Galerkin time discretization is *A*-stable only.

- The automatic adaptation of the space and time mesh is simplified by separating the errors of temporal and spatial discretization similar to the approach given in [6, 30]. For the coupled system (1.3), (1.4) and convection-dominated transport, that is captured here by the application of the **Streamline Upwind Petrov–Galerkin** approach (cf., e.g., [28]), this separation becomes more involved since the spatial error representation is then depending on additional stabilization terms; cf., e.g. [6], where the nonstationary Navier-Stokes equations along with local projection stabilization (LPS) is investigated for Péclet numbers up to a magnitude of  $10^3$ . Further, the additional numerical approximation of the flow field requires the consideration of additional terms within the derivation of the DWR localized error representation.
- The treatment of the dual residual in the error representation of the DWR approach differs throughout the literature. Often (cf., e.g., [4]) the dual residual is rewritten in terms of the primal residual plus some higher-order perturbations of the error in the goal quantity. Similarly to, e.g., [6, 30], this is no longer done here. In this work, the dual residual is computed explicitly for both error representations, the error in space and time, in addition to the primal residual.
- For this work a new software based on tensor-product space-time slabs was developed. This is an extension of the software used in [22]. In the software platform a tensor product of the  $d$ -dimensional spatial finite element space with an one-dimensional temporal finite element space is implemented. The temporal finite element space is based on a discontinuous Galerkin method of arbitrary order  $r$  on a one-dimensional triangulation. The temporal triangulation on a space-time slab is shared by the primal and dual problem. The temporal polynomial degree of the primal and dual problem can be chosen arbitrarily. These features enable the full space-time adaptivity and the flexible choice of polynomial degrees in space and time.
- Further, the software platform provides an encapsulated module for the flow solver (here the Stokes solver), that is coupled with fully adaptive solver of the transport equation and provides the flow field (convection coefficient). The latter needs to be interpolated from the flow (Stokes) solver to the adaptively refined spatial meshes on a slab of the transport problem. For the future, this concept enables the realization of multirate, fully space-time adaptive extensions of the current schemes and the incorporation of more sophisticated flow problems.

### 1.5. Outline

This work is organized as follows. In Sec. 2 we present the space-time discretization of our model problem, including its stabilization for convection-dominated transport. In Sec. 3 the DWR method is applied and localized a posteriori error representations, separating the effects of temporal and spatial discretization, are derived. In Sec. 4 the adaptive algorithm for automatic mesh refinement and the data structure of our implementation of the DWR based space-time adaptivity in the deal.II library are presented. Finally, in Sec. 5 its numerical performance properties are studied in a convergence test and illustrated for a sophisticated test setting. We end with conclusions.

Our notation for Sobolev and Bochner spaces is standard. The notation of the discretization in time and space is introduced below in Sec. 2.

## 2. Stabilized space-time discretization

In this section we briefly introduce the space-time finite element discretization of (1.3), (1.4) including the SUPG stabilization to capture convection-dominated transport.

### 2.1. Weak formulation

Let  $X := \{v \in L^2(0, T; H_0^1(\Omega)) \mid \partial_t v \in L^2(0, T; H^{-1}(\Omega))\}$ . The weak formulation of (1.4) reads as follows: Find  $u \in X$ , such that

$$A(u)(\varphi) = G(\varphi) \quad \forall \varphi \in X, \quad (2.1)$$

where the bilinear form  $A : X \times X \rightarrow \mathbb{R}$  and the linear form  $G : L^2(0, T; H^{-1}(\Omega)) \rightarrow \mathbb{R}$  are defined by

$$\begin{aligned} A(u)(\varphi) &:= \int_I \{(\rho \partial_t u, \varphi) + a(u)(\varphi)\} dt + (u(0), \varphi(0)), \\ G(\varphi) &:= \int_I (g, \varphi) dt + (u_0, \varphi(0)), \end{aligned}$$

with the bilinear form  $a : H_0^1(\Omega) \times H_0^1(\Omega) \rightarrow \mathbb{R}$  given by

$$a(u)(\varphi) := (\varepsilon \nabla u, \nabla \varphi) + (\mathbf{v} \cdot \nabla u, \varphi) + (\alpha u, \varphi). \quad (2.3)$$

Here,  $(\cdot, \cdot)$  denotes the inner product of  $L^2(\Omega)$  or duality pairing of  $H^{-1}(\Omega)$  with  $H_0^1(\Omega)$ , respectively. By  $\|\cdot\|$  we denote the associated  $L^2$ -norm.

For the variational formulation of problem (1.3) we define  $L_0^2(\Omega) := \{p \in L^2(\Omega) \mid \int_{\Omega} p \, d\mathbf{x} = 0\}$ . Then we get: *For  $\mathbf{f} \in H^{-1}(\Omega)$  find  $\{\mathbf{v}, p\} \in Y := H_0^1(\Omega)^d \times L_0^2(\Omega)$ , such that*

$$B(\mathbf{v}, p)(\boldsymbol{\psi}, \chi) = F(\boldsymbol{\psi}) \quad \forall \{\boldsymbol{\psi}, \chi\} \in Y, \quad (2.4)$$

where the bilinear form  $B : Y \times Y \rightarrow \mathbb{R}$  and the linear form  $F : H^{-1}(\Omega) \rightarrow \mathbb{R}$  are defined by

$$B(\mathbf{v}, p)(\boldsymbol{\psi}, \chi) := \nu(\nabla \mathbf{v}, \nabla \boldsymbol{\psi}) - (p, \nabla \cdot \boldsymbol{\psi}) + (\nabla \cdot \mathbf{v}, \chi), \quad (2.5a)$$

$$F(\boldsymbol{\psi}) := (\mathbf{f}, \boldsymbol{\psi}). \quad (2.5b)$$

To simplify the notation, we denote by  $H^{-1}(\Omega)$  the dual space of  $H_0^1(\Omega)$  and  $H_0^1(\Omega)^d$ , respectively. The meaning is always clear from the context.

## 2.2. Discretization in Time

For the discretization in time of the transport problem (2.1) we use a discontinuous Galerkin method dG( $r$ ) with an arbitrary polynomial degree  $r \geq 0$ . Let  $0 =: t_0 < t_1 < \dots < t_N := T$  be a partition of the closure of the time domain  $\bar{I} = [0, T]$  into left-open subintervals  $I_n := (t_{n-1}, t_n]$ ,  $n = 1, \dots, N$ , with time step sizes  $\tau_n = t_n - t_{n-1}$  and the global time discretization parameter  $\tau = \max_n \tau_n$ . Therefore, we introduce the time-discrete function space  $X_{\tau}^{\text{dG}(r)}$  for the transport problem.

$$X_{\tau}^{\text{dG}(r)} := \left\{ u_{\tau} \in L^2(I; H_0^1(\Omega)) \mid u_{\tau}|_{I_n} \in \mathcal{P}_r(I_n; H_0^1(\Omega)), \right. \\ \left. u_{\tau}(0) \in L^2(\Omega), n = 1, \dots, N \right\}, \quad (2.6)$$

where  $\mathcal{P}_r(\bar{I}_n; H_0^1(\Omega))$  denotes the space of all polynomials in time up to degree  $r \geq 0$  on  $I_n$  with values in  $H_0^1(\Omega)$ .

For some discontinuous in time function  $u_{\tau} \in X_{\tau}^{\text{dG}(r)}$  we define the limits  $u_{\tau, n}^{\pm}$  from above and below of  $u_{\tau}$  at  $t_n$  as well as their jump at  $t_n$  by

$$u_{\tau, n}^{\pm} := \lim_{t \rightarrow t_n \pm 0} u_{\tau}(t), \quad [u_{\tau}]_n := u_{\tau, n}^{+} - u_{\tau, n}^{-}.$$

The semidiscretization in time of the the transport problem (2.1) then reads as follows: *Find  $u_{\tau} \in X_{\tau}^{\text{dG}(r)}$  such that*

$$A_{\tau}(u_{\tau})(\varphi_{\tau}) = G_{\tau}(\varphi_{\tau}) \quad \forall \varphi_{\tau} \in X_{\tau}^{\text{dG}(r)}, \quad (2.7)$$

where the semi-discrete bilinear form and linear form are given by

$$A_{\tau}(u_{\tau})(\varphi_{\tau}) := \sum_{n=1}^N \int_{I_n} \{(\rho \partial_t u_{\tau}, \varphi_{\tau}) + a(u_{\tau})(\varphi_{\tau})\} dt \\ + \sum_{n=2}^N (\rho [u_{\tau}]_{n-1}, \varphi_{\tau, n-1}^{+}) + (\rho u_{\tau, 0}^{+}, \varphi_{\tau, 0}^{+}), \quad (2.8a)$$

$$G_{\tau}(\varphi_{\tau}) := \int_I (g, \varphi_{\tau}) \, dt + (u_0, \varphi_{\tau, 0}^{+}). \quad (2.8b)$$

## 2.3. Discretization in Space

Next, we describe the Galerkin finite element approximation in space of the semi-discrete transport problem (2.7) and the flow problem (2.4), respectively. We use Lagrange type finite element spaces of continuous functions that are piecewise polynomials. For the discretization in space, we consider a decomposition  $\mathcal{T}_h$  of the domain  $\Omega$  into disjoint elements  $K$ , such that  $\bar{\Omega} = \cup_{K \in \mathcal{T}_h} \bar{K}$ . Here, we choose the elements  $K \in \mathcal{T}_h$  to be quadrilaterals for  $d = 2$  and hexahedrals for  $d = 3$ . We denote by  $h_K$  the diameter of the element  $K$ . The global space discretization parameter  $h$  is given by  $h := \max_{K \in \mathcal{T}_h} h_K$ . Our mesh adaptation process yields locally refined cells, which is enabled by using hanging nodes. We point out that the global conformity of the finite element approach is preserved since the unknowns at such hanging nodes are eliminated by interpolation between the neighboring 'regular' nodes; cf. [4, Chapter 4.2] and [11] for more details. On  $\mathcal{T}_h$  we define the discrete finite element space by  $V_h^{p, n} := \{v \in C(\bar{\Omega}) \mid v|_K \in Q_h^p(K), \forall K \in \mathcal{T}_h\}$ , with  $n = 1, \dots, N$ , where  $Q_h^p(K)$  where  $\mathbb{Q}_r(K)$  is the space defined by the multilinear reference mapping of polynomials on the reference element with

maximum degree  $p$  in each variable. By replacing  $H_0^1(\Omega)$  in the definition of the semi-discrete function space  $X_\tau^{\text{dG}(r)}$  in (2.6) by  $V_h^{p,n}$ , we obtain the fully discrete function space for the transport problem

$$X_{\tau h}^{\text{dG}(r),p} := \left\{ u_{\tau h} \in X_\tau^{\text{dG}(r)} \mid u_{\tau h}|_{I_n} \in \mathcal{P}_r(I_n; H_h^{p_u,n}), \right. \\ \left. u_{\tau h}(0) \in H_h^{p_u,0}, n = 1, \dots, N \right\} \subseteq L^2(I; H_0^1(\Omega)). \quad (2.9)$$

The discrete in space function space for the flow problem is given by

$$Y_h^p := (H_h^{p_v})^d \times L_h^{p_p} \subseteq Y, \quad (2.10)$$

$$H_h^{p_u,n} := V_h^{p_u,n} \cap H_0^1(\Omega), \quad H_h^{p_v} := V_h^{p_v} \cap H_0^1(\Omega), \quad L_h^{p_p} := V_h^{p_p} \cap L_0^2(\Omega).$$

We note that the spatial finite element space  $V_h^{p,n}$  is allowed to be different on all subintervals  $I_n$  which is natural in the context of a discontinuous Galerkin approximation of the time variable and allows dynamic mesh changes in time. Due to the conformity of  $H_h^{p_u,n}$  we get  $X_{\tau h}^{\text{dG}(r),p} \subseteq X_\tau^{\text{dG}(r)}$ .

The fully discrete scheme for the flow problem then reads as follows: *Find*  $\{\mathbf{v}_h, p_h\} \in Y_h^p$  *such that*

$$B(\mathbf{v}_h, p_h)(\psi_h, \chi_h) = F(\psi_h) \quad \forall \{\psi_h, \chi_h\} \in Y_h^p, \quad (2.11)$$

*with*  $B(\cdot, \cdot)(\cdot, \cdot)$  *and*  $F(\cdot)$  *being defined in (2.5a) and (2.5b), respectively.*

The fully discrete discontinuous in time scheme for the transport problem then reads as follows: *Find*  $u_{\tau h} \in X_{\tau h}^{\text{dG}(r),p}$  *such that*

$$A_{\tau h}(u_{\tau h})(\varphi_{\tau h}) = G_\tau(\varphi_{\tau h}) \quad \forall \varphi_{\tau h} \in X_{\tau h}^{\text{dG}(r),p}, \quad (2.12)$$

*with*  $A_{\tau h}(\cdot)(\cdot)$  *and*  $G_\tau(\cdot)$  *being defined in (2.7) and (2.8b), respectively.* We note that the bilinear form  $a_h(u_{\tau h})(\varphi_{\tau h})$  in  $A_{\tau h}(\cdot)(\cdot)$  is now defined by

$$a_h(u_{\tau h})(\varphi_{\tau h}) := (\varepsilon \nabla u_{\tau h}, \nabla \varphi_{\tau h}) + (\mathbf{v}_h \cdot \nabla u_{\tau h}, \varphi_{\tau h}) + (\alpha u_{\tau h}, \varphi_{\tau h}) \quad (2.13)$$

with the discrete velocity field  $\mathbf{v}_h \in (H_h^{p_v})^d$  replacing its continuous counterpart  $\mathbf{v} \in (H_0^1(\Omega))^d$ .

#### 2.4. SUPG Stabilization

In this work we consider, for the sake for physical realism, convection-dominated transport with small diffusion parameter  $\varepsilon$  in (1.4) which, on the hand, poses an additional challenge to the a posteriori error control but, on the other hand, illustrates nicely the potential, reliability and efficiency of the DWR-based approach. For convection-dominated transport, the finite element approximation needs is stabilized in order to further reduce spurious and non-physical oscillations of the discrete solution arising close to sharp fronts or layers. Here, we apply the streamline upwind Petrov-Galerkin method (for short SUPG); cf. [17, 8, 28, 20]. We explicitly note that SUPG stabilization and automatic mesh adaptation interact strongly (cf. also Remark 2.1). Balancing their effects needs particular consideration (cf. [10]) and has not been strongly studied so far in the literature.

The stabilized variant of the fully discrete scheme (2.12) then reads as follows: *Find*  $u_{\tau h} \in X_{\tau h}^{\text{dG}(r),p}$  *such that*

$$A_S(u_{\tau h})(\varphi_{\tau h}) = G_\tau(\varphi_{\tau h}) \quad \forall \varphi_{\tau h} \in X_{\tau h}^{\text{dG}(r),p}, \quad (2.14)$$

*with*  $A_S(u_{\tau h})(\varphi_{\tau h}) := A_{\tau h}(u_{\tau h})(\varphi_{\tau h}) + S(u_{\tau h})(\varphi_{\tau h})$  *and stabilization term*

$$S(u_{\tau h})(\varphi_{\tau h}) := \sum_{n=1}^N \int_{I_n} \sum_{K \in \mathcal{T}_h} \delta_K(r(u_{\tau h}), \mathbf{v}_h \cdot \nabla \varphi_{\tau h})_K \, dt \\ + \sum_{n=2}^N \sum_{K \in \mathcal{T}_h} \delta_K(\rho[u_{\tau h}]_{n-1}, \mathbf{v}_h \cdot \nabla \varphi_{\tau h, n-1}^+)_K \\ + \sum_{K \in \mathcal{T}_h} \delta_K(\rho u_{\tau h, 0}^+ - u_0, \mathbf{v}_h \cdot \nabla \varphi_{\tau h, 0}^+)_K \quad (2.15)$$

*and residual*

$$r(u_{\tau h}) := \rho \partial_t u_{\tau h} - \nabla \cdot (\varepsilon \nabla u_{\tau h}) + \mathbf{v}_h \cdot \nabla u_{\tau h} + \alpha u_{\tau h} - g.$$

**Remark 2.1.** The proper choice of the stabilization parameter  $\delta_K$  is an important issue in the application of the SUPG approach; cf., e.g., [18] and the discussion therein. For time-dependent convection-diffusion-reaction problems an optimal error estimate for  $\delta_K = O(h)$  is derived in [18].

**Remark 2.2.** For the error  $e = u_\tau - u_{\tau h}$  we get by subtracting Eq. (2.14) from Eq. (2.7) the identity

$$\begin{aligned} & \sum_{n=1}^N \int_{I_n} \{(\rho \partial_t e, \varphi_{\tau h}) + a_h(e)(\varphi_{\tau h})\} dt \\ & \quad + \sum_{n=2}^N (\rho[e]_{n-1}, \varphi_{\tau h, n-1}^+) + (e_0^+, \varphi_{\tau h, 0}^+) \\ & = S(u_{\tau h})(\varphi_{\tau h}) - \sum_{n=1}^N \int_{I_n} ((\mathbf{v} - \mathbf{v}_h) \cdot \nabla u_\tau, \varphi_{\tau h}) dt, \end{aligned} \quad (2.16)$$

with a non-vanishing right-hand side term depending on the stabilization and the error in the approximation of the flow field. Eq. (2.16) with the perturbation term on the right-hand side replaces the standard Galerkin orthogonality of the space-time finite element approximation.

### 3. A Posteriori error estimation

In this section we derive our DWR error representation for the coupled system (2.11), (2.14). In this work, only goal quantities depending on the unknown  $u$  are studied. For applications of practical interest, physical quantities in terms of the transport quantity  $u$  are typically of higher relevance than quantities in the unknowns  $\mathbf{v}$  and  $p$  of the flow problem. In the sequel, we denote by  $J : X \rightarrow \mathbb{R}$  a user-chosen, physically relevant target functional represented in the form

$$J(u) = \int_0^T J_1(u(t)) dt + J_2(u(T)), \quad (3.1)$$

where  $J_1 : H_0^1(\Omega) \rightarrow \mathbb{R}$  or  $J_2 : H_0^1(\Omega) \rightarrow \mathbb{R}$  may be zero. Since we aim at controlling the respective errors due to the discretization in time as well as in space, we split the a posteriori error representation with respect to  $J$  into the contributions

$$J(u) - J(u_{\tau h}) = J(u) - J(u_\tau) + J(u_\tau) - J(u_{\tau h}). \quad (3.2)$$

For the respective error representations we define the Lagrangian functionals  $\mathcal{L} : X \times X \rightarrow \mathbb{R}$ ,  $\mathcal{L}_\tau : X_\tau^{\text{dG}(r)} \times X_\tau^{\text{dG}(r)} \rightarrow \mathbb{R}$ , and  $\mathcal{L}_{\tau h} : X_{\tau h}^{\text{dG}(r), p} \times X_{\tau h}^{\text{dG}(r), p} \rightarrow \mathbb{R}$  by

$$\mathcal{L}(u, z) := J(u) + G_\tau(z) - A(u)(z), \quad (3.3a)$$

$$\mathcal{L}_\tau(u_\tau, z_\tau) := J(u_\tau) + G_\tau(z_\tau) - A_\tau(u_\tau)(z_\tau), \quad (3.3b)$$

$$\mathcal{L}_{\tau h}(u_{\tau h}, z_{\tau h}) := J(u_{\tau h}) + G_\tau(z_{\tau h}) - A_S(u_{\tau h})(z_{\tau h}). \quad (3.3c)$$

Here, the Lagrange multipliers  $z$ ,  $z_\tau$ , and  $z_{\tau h}$  are called *dual variables* in contrast to the primal variables  $u$ ,  $u_\tau$ , and  $u_{\tau h}$ ; cf. [6, 5]. Considering the directional derivatives of the Lagrangian functionals, also known as Gâteaux derivatives, with respect to their first argument, i.e.

$$\mathcal{L}'_z(u, z)(\varphi) := \lim_{t \neq 0, t \rightarrow 0} t^{-1} \{ \mathcal{L}(u, z + t\varphi) - \mathcal{L}(u, z) \}, \quad \varphi \in X, \quad (3.4)$$

leads to the so-called dual problems [6]. The continuous, semi-discrete, and fully discrete dual solutions  $z \in X$ ,  $z_\tau \in X_\tau^{\text{dG}(r)}$ , and  $z_{\tau h} \in X_{\tau h}^{\text{dG}(r), p}$  are thus determined by the optimality conditions

$$\mathcal{L}'_u(u, z)(\varphi) = 0 \quad \forall \varphi \in X, \quad (3.5a)$$

$$\mathcal{L}'_{\tau, u}(u_\tau, z_\tau)(\varphi) = 0 \quad \forall \varphi_\tau \in X_\tau^{\text{dG}(r)}, \quad (3.5b)$$

$$\mathcal{L}'_{\tau h, u}(u_{\tau h}, z_{\tau h})(\varphi) = 0 \quad \forall \varphi_{\tau h} \in X_{\tau h}^{\text{dG}(r), p}. \quad (3.5c)$$

More precisely, the continuous dual solution  $z \in X$  is the solution of

$$A'(u)(\varphi, z) = J'(u)(\varphi) \quad \forall \varphi \in X, \quad (3.6)$$

where the adjoint bilinear form  $A'$  is given by

$$A'(u)(\varphi, z) := \int_I \{(\varphi, -\rho \partial_t z) + a'(u)(\varphi, z)\} dt + (\varphi(T), z(T)).$$

We note that for the representation (3) of  $A'$  integration by parts in time is applied, which is allowed for weak solutions  $z \in X$ ; cf., e.g., [27, Lemma 8.9]. The derivative  $a'(u)(\varphi, z)$  of the bilinear form  $a(u)(z)$  in  $A'$  admits the explicit form

$$a'(u)(\varphi, z) = (\varepsilon \nabla \varphi, \nabla z) + (\mathbf{v} \cdot \nabla \varphi, z) + (\alpha \varphi, z).$$

The right-hand side of Eq. (3.6) is given by

$$J'(u)(\varphi) := \int_I J'_1(u)(\varphi) dt + J'_2(u(T))(\varphi(T)). \quad (3.7)$$

Further, the semi-discrete dual solution  $z_\tau \in X_\tau^{\text{dG}(r)}$  and the fully discrete dual solution  $z_{\tau h} \in X_{\tau h}^{\text{dG}(r),p}$  satisfy the equations

$$A'_\tau(u_\tau)(\varphi_\tau, z_\tau) = J'(u_\tau)(\varphi_\tau) \quad \forall \varphi_\tau \in X_\tau^{\text{dG}(r)}, \quad (3.8a)$$

$$A'_S(u_{\tau h})(\varphi_{\tau h}, z_{\tau h}) = J'(u_{\tau h})(\varphi_{\tau h}) \quad \forall \varphi_{\tau h} \in X_{\tau h}^{\text{dG}(r),p}, \quad (3.8b)$$

where  $A'_\tau$  and  $A'_S$  are given by

$$\begin{aligned} A'_\tau(u_\tau)(\varphi_\tau, z_\tau) := & \sum_{n=1}^N \int_{I_n} \{(\varphi_\tau, -\rho \partial_t z_\tau) + a'(u_\tau)(\varphi_\tau, z_\tau)\} dt \\ & - \sum_{n=1}^{N-1} (\varphi_{\tau,n}^-, \rho[z_\tau]_n) + (\varphi_{\tau,N}^-, \rho z_{\tau,N}^-), \end{aligned}$$

and

$$\begin{aligned} A'_S(u_{\tau h})(\varphi_{\tau h}, z_{\tau h}) := & \sum_{n=1}^N \int_{I_n} \{(\varphi_{\tau h}, -\rho \partial_t z_{\tau h}) + a'_h(u_{\tau h})(\varphi_{\tau h}, z_{\tau h})\} dt \\ & + S'(u_{\tau h})(\varphi_{\tau h}, z_{\tau h}) - \sum_{n=1}^{N-1} (\varphi_{\tau h,n}^-, \rho[z_{\tau h}]_n) + (\varphi_{\tau h,N}^-, \rho z_{\tau h,N}^-). \end{aligned}$$

**Remark 3.1.** We note that the directional derivatives of the Lagrangian functionals with respect to their second argument leads to the primal problems given by Eqs. (2.1), (2.7) and (2.14), respectively.

For the derivation of computable representations of the separated error contributions in Eq. (3.2) we need the following known result, that is explicitly summarized here in order to keep this work self-contained.

**Lemma 3.1.** *Let  $\mathcal{Y}$  be a function space and  $L$  and  $\tilde{L}$  be three times Gâteaux differentiable functionals on  $\mathcal{Y}$ . We seek a stationary point  $y_1$  of  $L$  on a subspace  $\mathcal{Y}_1 \subseteq \mathcal{Y}$ : Find  $y_1 \in \mathcal{Y}_1$  such that*

$$L'(y_1)(\delta y_1) = 0 \quad \forall \delta y_1 \in \mathcal{Y}_1. \quad (3.9)$$

*This equation is approximated by a Galerkin method using the functional  $\tilde{L}$  on a subspace  $\mathcal{Y}_2 \subseteq \mathcal{Y}$ . Hence, the discrete problem seeks  $y_2 \in \mathcal{Y}_2$  such that*

$$\tilde{L}'(y_2)(\delta y_2) = 0 \quad \forall \delta y_2 \in \mathcal{Y}_2. \quad (3.10)$$

*If the continuous solution  $y_1$  additionally fulfills*

$$L'(y_1)(y_2) = 0, \quad (3.11)$$

*with the approximated solution  $y_2$ , we have the error representation*

$$\begin{aligned} L(y_1) - \tilde{L}(y_2) = & \frac{1}{2} L'(y_2)(y_1 - \tilde{y}_2) \\ & + \frac{1}{2} (L - \tilde{L})'(y_2)(\tilde{y}_2 - y_2) + (L - \tilde{L})(y_2) + \mathcal{R}, \end{aligned} \quad (3.12)$$

*for arbitrary  $\tilde{y}_2 \in \mathcal{Y}_2$ , where the remainder term  $\mathcal{R}$  is given in terms of  $e := y_1 - y_2$  as*

$$\mathcal{R} = \frac{1}{2} \int_0^1 L'''(y_2 + se)(e, e, e) s(s-1) ds. \quad (3.13)$$

*Proof.* The proof of Lemma 3.1 can be found in [6]. □

In the following Thm. 3.1 we apply the abstract error representation formula (3.12) to the Lagrangian functionals (3.3a)–(3.3c). This step is a modification of Thm. 5.2 in [6] due to the presence of the additional coupling term. To proceed with our computations, we still introduce the primal and dual residuals that are defined by means of

$$\rho_t(u)(\varphi) := \mathcal{L}'_{\tau,z}(u, z)(\varphi), \quad \rho_t^*(u, z)(\varphi) := \mathcal{L}'_{\tau,u}(u, z)(\varphi). \quad (3.14)$$

By using Lemma 3.1 we now get the following result for the DWR-based error representation.



**Theorem 3.1.** Let  $\{u, z\} \in X \times X$ ,  $\{u_\tau, z_\tau\} \in X_\tau^{\text{dG}(r)} \times X_\tau^{\text{dG}(r)}$ , and  $\{u_{\tau h}, z_{\tau h}\} \in X_{\tau h}^{\text{dG}(r),p} \times X_{\tau h}^{\text{dG}(r),p}$  denote the stationary points of  $\mathcal{L}$ ,  $\mathcal{L}_\tau$ , and  $\mathcal{L}_{\tau h}$  on the different levels of discretization, i.e.,

$$\begin{aligned}\mathcal{L}'(u, z)(\delta u, \delta z) &= \mathcal{L}'_\tau(u, z)(\delta u, \delta z) = 0 \quad \forall \{\delta u, \delta z\} \in X \times X, \\ \mathcal{L}'_\tau(u_\tau, z_\tau)(\delta u_\tau, \delta z_\tau) &= 0 \quad \forall \{\delta u_\tau, \delta z_\tau\} \in X_\tau^{\text{dG}(r)} \times X_\tau^{\text{dG}(r)}, \\ \mathcal{L}'_{\tau h}(u_{\tau h}, z_{\tau h})(\delta u_{\tau h}, \delta z_{\tau h}) &= 0 \quad \forall \{\delta u_{\tau h}, \delta z_{\tau h}\} \in X_{\tau h}^{\text{dG}(r),p} \times X_{\tau h}^{\text{dG}(r),p}.\end{aligned}$$

Additionally, for the error  $e = u_\tau - u_{\tau h}$  we have the equation (2.16) of Galerkin orthogonality type. Then, for the discretization errors in space and time we get the representation formulas

$$J(u) - J(u_\tau) = \frac{1}{2}\rho_t(u_\tau)(z - \tilde{z}_\tau) + \frac{1}{2}\rho_t^*(u_\tau, z_\tau)(u - \tilde{u}_\tau) + \mathcal{R}_\tau, \quad (3.15a)$$

$$\begin{aligned}J(u_\tau) - J(u_{\tau h}) &= \frac{1}{2}\rho_t(u_{\tau h})(z_\tau - \tilde{z}_{\tau h}) + \frac{1}{2}\rho_t^*(u_{\tau h}, z_{\tau h})(u_\tau - \tilde{u}_{\tau h}) \\ &\quad + \frac{1}{2}\mathcal{D}'_{\tau h}(u_{\tau h}, z_{\tau h})(\tilde{u}_{\tau h} - u_{\tau h}, \tilde{z}_{\tau h} - z_{\tau h}) \\ &\quad + \mathcal{D}_{\tau h}(u_{\tau h}, z_{\tau h}) + \mathcal{R}_h,\end{aligned} \quad (3.15b)$$

where  $\mathcal{D}_{\tau h}(\cdot, \cdot)$  is given by

$$\mathcal{D}_{\tau h}(\varphi, \psi) = S(\varphi)(\psi) - \sum_{n=1}^N \int_{I_n} ((\mathbf{v} - \mathbf{v}_h) \cdot \nabla \varphi, \psi) dt, \quad (3.16)$$

with  $S(\cdot)(\cdot)$  being defined in (2.15). Here,  $\{\tilde{u}_\tau, \tilde{z}_\tau\} \in X_\tau^{\text{dG}(r)} \times X_\tau^{\text{dG}(r)}$ , and  $\{\tilde{u}_{\tau h}, \tilde{z}_{\tau h}\} \in X_{\tau h}^{\text{dG}(r),p} \times X_{\tau h}^{\text{dG}(r),p}$  can be chosen arbitrarily and the remainder terms  $\mathcal{R}_\tau$  and  $\mathcal{R}_h$  have the same structure as the remainder term (3.13) in Lemma 3.1.

*Proof.* The proof is related to that one of Thm. 5.2 in [6]. Evaluating the Lagrangian functionals at the respective primal and dual solutions, there holds that

$$J(u) = \mathcal{L}(u, z), \quad J(u_\tau) = \mathcal{L}_\tau(u_\tau, z_\tau), \quad J(u_{\tau h}) = \mathcal{L}_{\tau h}(u_{\tau h}, z_{\tau h}).$$

Since the additional jump terms in  $\mathcal{L}_\tau$  vanish for a continuous solution  $u \in X$ , we get the following representation for the temporal and spatial error, respectively,

$$J(u) - J(u_\tau) = \mathcal{L}(u, z) - \mathcal{L}_\tau(u_\tau, z_\tau) = \mathcal{L}_\tau(u, z) - \mathcal{L}_\tau(u_\tau, z_\tau), \quad (3.17a)$$

$$J(u_\tau) - J(u_{\tau h}) = \mathcal{L}_\tau(u_\tau, z_\tau) - \mathcal{L}_{\tau h}(u_{\tau h}, z_{\tau h}). \quad (3.17b)$$

To prove the assertion (3.15a) for the temporal error, we apply Lemma 3.1 with the identifications

$$L = \mathcal{L}_\tau, \quad \tilde{L} = \mathcal{L}_\tau, \quad \mathcal{Y}_1 = X \times X, \quad \mathcal{Y}_2 = X_\tau^{\text{dG}(r)} \times X_\tau^{\text{dG}(r)}.$$

to the identity (3.17a). Further, we have to choose  $\mathcal{Y} := \mathcal{Y}_1 + \mathcal{Y}_2$  since here  $X_\tau^{\text{dG}(r)} \not\subseteq X$ . Thus, we have to verify condition (3.11), that now reads as  $\mathcal{L}'(u, z)(u_\tau, z_\tau) = 0$ , or equivalently,

$$\mathcal{L}'_u(u, z)(u_\tau) = 0 \quad \text{and} \quad \mathcal{L}'_z(u, z)(z_\tau) = 0. \quad (3.18)$$

We only give the proof of the second equation in (3.18). The first one can be proved analogously. To show that  $\mathcal{L}'_z(u, z)(z_\tau) = 0$ , we rewrite Eq. (3.18) as

$$\sum_{n=1}^N \int_{I_n} \{(g - \rho \partial_t u, z_\tau) - a(u)(z_\tau)\} dt = 0.$$

By construction, the continuous solution  $u$  satisfies that

$$\int_I \{(\rho \partial_t u, \varphi) + a(u)(\varphi)\} dt = \int_I (g, \varphi) dt \quad \forall \varphi \in X. \quad (3.19)$$

Since  $X$  is dense in  $L^2(I; H_0^1(\Omega))$  with respect to the norm of  $L^2(I; H_0^1(\Omega))$  and since no time derivatives of  $\varphi$  arise in (3.19), this equation is also satisfied for all  $\varphi \in L^2(I; H_0^1(\Omega))$ . The inclusion  $z_\tau \in X_\tau^{\text{dG}(r)} \subset L^2(I; H_0^1(\Omega))$  then implies that the second equation in (3.18) is fulfilled.

Now, applying Lemma 3.1 with the above-made identifications yields that

$$\begin{aligned} J(u) - J(u_\tau) &= \mathcal{L}_\tau(u, z) - \mathcal{L}_\tau(u_\tau, z_\tau) \\ &= \frac{1}{2} \mathcal{L}'_\tau(u_\tau, z_\tau)(u - \tilde{u}_\tau, z - \tilde{z}_\tau) + \mathcal{R}_\tau. \end{aligned} \quad (3.20)$$

With the definition of the primal and dual residuals given in (3.14), Eq.(3.20) can be rewritten as

$$J(u) - J(u_\tau) = \frac{1}{2} \rho_t(u_\tau)(z - \tilde{z}_\tau) + \frac{1}{2} \rho_t^*(u_\tau, z_\tau)(u - \tilde{u}_\tau) + \mathcal{R}_\tau,$$

where the remainder term  $\mathcal{R}_\tau$  is given by

$$\mathcal{R}_\tau = \frac{1}{2} \int_0^1 \mathcal{L}'''_\tau(u_\tau + se, z_\tau + se^*)(e, e, e, e^*, e^*, e^*) s(s-1) ds,$$

with the ‘primal’ and ‘dual’ errors  $e := u - u_\tau$  and  $e^* := z - z_\tau$ , respectively. This proves the assertion (3.15a).

To prove the spatial error representation (3.15b), we apply Lemma 3.1 with the identifications

$$L = \mathcal{L}_\tau, \quad \tilde{L} = \mathcal{L}_{\tau h}, \quad \mathcal{Y}_1 = X_\tau^{\text{dG}(r)} \times X_\tau^{\text{dG}(r)}, \quad \mathcal{Y}_2 = X_{\tau h}^{\text{dG}(r),p} \times X_{\tau h}^{\text{dG}(r),p}$$

to Eq. (3.17b). In this case, we have  $\mathcal{Y}_2 \subseteq \mathcal{Y}_1$  since  $X_{\tau h}^{\text{dG}(r),p} \subseteq X_\tau^{\text{dG}(r)}$ . Hence, we can choose  $\mathcal{Y} := \mathcal{Y}_1$  in Lemma 3.1 and condition (3.11) is directly satisfied. Now, applying Lemma 3.1 with these identifications implies that

$$\begin{aligned} J(u_\tau) - J(u_{\tau h}) &= \mathcal{L}_\tau(u_\tau, z_\tau) - \mathcal{L}_{\tau h}(u_{\tau h}, z_{\tau h}) \\ &= \frac{1}{2} \mathcal{L}'_\tau(u_{\tau h}, z_{\tau h})(u_\tau - \tilde{u}_{\tau h}, z_\tau - \tilde{z}_{\tau h}) \\ &\quad + \frac{1}{2} (\mathcal{L}_\tau - \mathcal{L}_{\tau h})'(u_{\tau h}, z_{\tau h})(\tilde{u}_{\tau h} - u_{\tau h}, \tilde{z}_{\tau h} - z_{\tau h}) \\ &\quad + (\mathcal{L}_\tau - \mathcal{L}_{\tau h})(u_{\tau h}, z_{\tau h}) + \mathcal{R}_h. \end{aligned} \quad (3.21)$$

Again, using the definition in (3.14) of the primal and dual residual as well as the definition of  $\mathcal{D}_{\tau h}$  given by Eq. (3.16), Eq. (3.21) can be rewritten as

$$\begin{aligned} J(u_\tau) - J(u_{\tau h}) &= \frac{1}{2} \rho_t(u_{\tau h})(z_\tau - \tilde{z}_{\tau h}) + \frac{1}{2} \rho_t^*(u_{\tau h}, z_{\tau h})(u_\tau - \tilde{u}_{\tau h}) \\ &\quad + \frac{1}{2} \mathcal{D}'_{\tau h}(u_{\tau h}, z_{\tau h})(\tilde{u}_{\tau h} - u_{\tau h}, \tilde{z}_{\tau h} - z_{\tau h}) \\ &\quad + \mathcal{D}_{\tau h}(u_{\tau h}, z_{\tau h}) + \mathcal{R}_h, \end{aligned}$$

where the remainder term  $\mathcal{R}_h$  is given by

$$\mathcal{R}_h = \frac{1}{2} \int_0^1 \mathcal{L}'''_\tau(u_{\tau h} + se, z_{\tau h} + se^*)(e, e, e, e^*, e^*, e^*) s(s-1) ds,$$

with the ‘primal’ and ‘dual’ errors  $e := u_\tau - u_{\tau h}$  and  $e^* := z_\tau - z_{\tau h}$ . This proves the assertion (3.15b).  $\square$

## 4. Practical Aspects

Here we present the underlying adaptive algorithm and illustrate some practical aspects for the realization of the adaptivity process. The definition of the (localized) error indicators in the algorithm is given in Subsec. 4.2.

### 4.1. Adaptive algorithm and software

Our space-time adaptivity and mesh refinement strategy uses the following algorithm.

---

#### Algorithm: goal-oriented space-time adaptivity

---

##### Initialization:

- Find the solutions  $\{\mathbf{v}_h, p_h\} \in Y_h^p$  of the Stokes flow problem (1.3).
- Generate the initial space-time slabs  $Q_n^1 = \Omega_h^{n,1} \times I_\tau^{n,1}$ ,  $n = 1, \dots, N^1$ , with  $\bar{I} = \cup_n \bar{I}_\tau^{n,1}$ , for the goal-oriented adaptive transport problem.

---

**DWR-loop**  $\ell = 1, \dots$ :

1. **Find the primal solution**  $u_{\tau h} \in X_{\tau h}^{\text{primal}}$  of problem (1.4).
  2. **Break if the goal yields convergence**, i.e. e.g.  $\|u - u_{\tau h}^\ell\| < \text{tol}$ .
  3. **Find the dual solution**  $z_{\tau h} \in X_{\tau h}^{\text{dual}}$  of problem (1.4).
  4. **Evaluate the a posteriori space-time error indicators**  $\eta_h$  and  $\eta_\tau$  given by Eq. (4.2) and (4.1), respectively.
  5. **Mark the slabs**  $Q_{\tilde{n}}^\ell$ ,  $\tilde{n} \in \{1, \dots, N^\ell\}$ , **for temporal refinement** if the corresponding  $\eta_\tau^{\tilde{n}}$  is in the set of  $\theta_\tau^{\text{top}}$  percent of the worst indicators.
  6. **Mark the cells**  $\tilde{K} \in \Omega_h^{n,\ell}$  **for spatial refinement** if the corresponding  $\eta_h^n|_{\tilde{K}}$  is in the set of  $\theta_h^{\text{top}}$  percent of the worst indicators, **or**, respectively, **mark for spatial coarsening** if  $\eta_h^n|_{\tilde{K}}$  is in the set of  $\theta_h^{\text{bottom}}$  percent of the best indicators.
  7. **Execute spatial adaptations** on all slabs under the use of mesh smoothing operators.
  8. **Execute temporal refinements of slabs**.
  9. Increase  $\ell$  to  $\ell + 1$  and return to Step 1.
- 

Regarding this algorithm, we note the following issues.

- Remark 4.1.** • The primal and dual spaces in the Steps 1 and 3 of the algorithm,  $X_{\tau h}^{\text{primal}} = X_{\tau h}^{\text{dG}(r), \text{cG}(p)}$  and  $X_{\tau h}^{\text{dual}} = X_{\tau h}^{\text{dG}(s), \text{cG}(q)}$ , must be chosen properly, i.e.  $p < q$  and  $r < s$ .
- Within the Steps 1, 3 and 4 of the algorithm, the computed convection field  $\mathbf{v}_h$  of the Stokes problem is interpolated to the adaptively refined spatial triangulation of the space-time slabs.
  - Technical details about the implementation of Step 7 and 8 are given in [22, Sec. 1.2].

A new software, the `dwr-stokes-condiffrea` module of the `DTM++` project, was developed for the implementation of the adaptive algorithm. The new module is an extension of the published open-source module `dwr-diffusion` of the `DTM++` project; cf. [22]. The extensions are the implementation of the space-time tensor-product finite element spaces for the primal and dual problem on each slab and the coupling of the transport solver to a separated flow module integrated in the software platform. This object-oriented software architecture facilitates future extensions and the usage of different and more sophisticated flow problems. Our simulation tools of the `DTM++` project are frontend solvers for the `deal.II` library; cf. [2].

#### 4.2. Local error indicators

Finally, we give some remarks regarding the localization of the error representations that are derived in Thm. 3.1. Their practical realization and the definition of *error indicators*  $\eta_\tau$  and  $\eta_h$  is obtained by neglecting the remainder terms  $\mathcal{R}_\tau$  and  $\mathcal{R}_h$  of the result given in Thm. 3.1 and splitting the resulting quantities into elementwise contributions.

$$\begin{aligned}
 J(u) - J(u_\tau) &\doteq \frac{1}{2} \rho_t^n(u_\tau)(z - \tilde{z}_\tau) + \frac{1}{2} \rho_t^{*,n}(u_\tau, z_\tau)(u - \tilde{u}_\tau) \\
 &=: \eta_\tau = \sum_{n=1}^N \eta_\tau^n,
 \end{aligned} \tag{4.1}$$

$$\begin{aligned}
 J(u_\tau) - J(u_{\tau h}) &\doteq \frac{1}{2} \rho_t^n(u_{\tau h})(z_\tau - \tilde{z}_{\tau h}) + \frac{1}{2} \rho_t^{*,n}(u_{\tau h}, z_{\tau h})(u_\tau - \tilde{u}_{\tau h}) \\
 &\quad + \frac{1}{2} \mathcal{D}_{\tau h}'^n(u_{\tau h}, z_{\tau h})(\tilde{u}_{\tau h} - u_{\tau h}, \tilde{z}_{\tau h} - z_{\tau h}) + \mathcal{D}_{\tau h}^n(u_{\tau h}, z_{\tau h}) \\
 &=: \eta_h = \sum_{n=0}^N \eta_h^n = \sum_{n=0}^N \sum_{K \in \mathcal{T}_h^n} \eta_{h,K}^n.
 \end{aligned} \tag{4.2}$$

To compute the error indicators  $\eta_\tau$  and  $\eta_h$  we replace all unknown solutions by the approximated fully discrete solutions  $u_{\tau h} \in X_{\tau h}^{\text{dG}(r), \text{cG}(p)}$  and  $z_{\tau h} \in X_{\tau h}^{\text{dG}(s), \text{cG}(q)}$ , with  $r < s$  and  $p < q$ , whereby the arising weights are approximated in the following way.

- We put  $u - \tilde{u}_\tau \approx E_\tau^{r+1}(u_{\tau h}) - u_{\tau h}$  with  $E_\tau^{r+1}(\cdot)$  denoting the extrapolation in time operator that acts on a time cell of length  $\tau$  and lifts the solution to a piecewise polynomial of degree  $(r+1)$  in time.

We note that the additional solution for the (local) extrapolation in time on a specific time cell is here interpolated from the previous time cell or the initial condition  $u_0$  in the left end of the time cell. For this, the previous time cell is located on the same slab  $Q_n^\ell$  or the previous one  $Q_{n-1}^\ell$ , where the latter case requires an additional interpolation between two spatial triangulations.

In future works, this concept can be extended to a patchwise higher-order extrapolation in time by using the solutions of two neighboring time cells with an order in time of  $(2r+1)$  on the  $2\tau$  patch time cell.

- We put  $u_\tau - \tilde{u}_{\tau h} \approx E_{2h}^{2p}(u_{\tau h}) - u_{\tau h}$ , with  $E_{2h}^{2p}(\cdot)$  denoting the extrapolation in space operator that acts on a patched cell of size  $2h$  and lifts the solution to a piecewise polynomial of degree  $2p$  on the reference cell corresponding to the patched cell of width  $2h$ .

We note that the extrapolation operator in space is implemented in the `deal.II` library for quadrilateral and hexahedral finite elements and continuous discrete functions of piecewise polynomials with degree  $p$  in each variable. The application of this operator of `deal.II` requires the spatial triangulation on each slab being at least once globally refined to construct the patched cells of size  $2h$ . Thereby, an extrapolation degree of at most  $2p$  (and not  $2p+1$ ) is due to the shared degrees of freedom on the edges or faces of the continuous FE solution.

- We put  $z - \tilde{z}_\tau \approx z_{\tau h} - R_\tau^r(z_{\tau h})$  with  $R_\tau^r(\cdot)$  denoting the restriction in time operator on a time cell that restricts the solution to a polynomial of degree  $r < s$ .

We note that the restriction operator in time is implemented in our software since `deal.II` is currently not able to operate on  $(d+1)$ -dimensional tensor-product solutions. This is done by a Lagrangian interpolation in time to the primal space of the dual solution and an additional reinterpolation to the dual space.

- We put  $z_\tau - \tilde{z}_{\tau h} \approx z_{\tau h} - R_h^p(z_{\tau h})$  with  $R_h^p(\cdot)$  denoting the restriction in space operator that acts on a spatial cell and restricts the solution to a polynomial of degree  $p < q$  on the corresponding reference cell.

We note that the restriction operator in space is implemented in the `deal.II` library for dimension  $d = 2, 3$  as back-interpolation operator (cf. [2] for details) between two finite element spaces that are here the dual finite element space and the intermediate primal finite element space.

The respective operators are chosen in the described manner, since for the dual problem we pursue and favor a *higher-order* approach, i.e., we use higher-order finite element methods in space and time, compared to those applied to the primal problem. Our motivation for this becomes from the results of a comparative study between higher-order interpolation and higher-order finite elements that has been done for a steady-state variant of a convection-dominated problem by two of the authors in [10].

For measuring the accuracy of the error estimator, we will study in our numerical convergence experiments (cf. Sec. 5.1) the effectivity index

$$\mathcal{I}_{\text{eff}} = \left| \frac{\eta_\tau + \eta_h}{J(u) - J(u_{\tau h})} \right| \quad (4.3)$$

as the ratio of the estimated error over the exact error. Desirably, the index  $\mathcal{I}_{\text{eff}}$  should be close to one.

## 5. Numerical Examples

In the following section we study the convergence, computational efficiency and stability of the introduced goal-oriented adaptivity approach for the coupled transport and flow problem. The first example in Sec. 5.1 is an academic problem with a given analytical solution to study the space-time higher-order convergence behavior with a constant convection field for a non-stabilized convection-diffusion transport and a stabilized convection-dominated transport. The lowest-order results can be compared with our preceding published works [10, 22]. The second example in Sec. 5.2 is motivated by problem of physical relevance in which we simulate a convection-dominated transport with goal-oriented adaptivity of a species through a channel with a constraint.

### 5.1. Example 1 (Stabilized higher-order space-time Convergence Studies)

This first example is an academic test problem with the given solution

$$\begin{aligned} u(\mathbf{x}, t) &:= u_1 \cdot u_2, \quad \mathbf{x} = (x_1, x_2)^\top \in \mathbb{R}^2 \text{ and } t \in \mathbb{R}, \\ u_1(\mathbf{x}, t) &:= (1 + a \cdot ((x_1 - m_1(t))^2 + (x_2 - m_2(t))^2))^{-1}, \\ u_2(t) &:= \nu_1(t) \cdot s \cdot \arctan(\nu_2(t)), \end{aligned} \quad (5.1)$$

with  $m_1(t) := \frac{1}{2} + \frac{1}{4} \cos(2\pi t)$  and  $m_2(t) := \frac{1}{2} + \frac{1}{4} \sin(2\pi t)$ , and,  $\nu_1(\hat{t}) := -1$ ,  $\nu_2(\hat{t}) := 5\pi \cdot (4\hat{t} - 1)$ , for  $\hat{t} \in [0, 0.5]$  and  $\nu_1(\hat{t}) := 1$ ,  $\nu_2(\hat{t}) := 5\pi \cdot (4(\hat{t} - 0.5) - 1)$ , for  $\hat{t} \in [0.5, 1]$ ,  $\hat{t} = t - k$ ,  $k \in \mathbb{N}_0$ , and, scalars  $a = 50$  and  $s = -\frac{1}{3}$ . The (analytic) solution (5.1) mimics a counterclockwise rotating cone which additionally changes its height and orientation over the period  $T = 1$ . Precisely, the orientation of the cone switches from negative to positive while passing  $t = 0.25$  and from positive to negative while passing  $t = 0.75$ . Exemplary solution profiles at  $t = 0$ ,  $t = 0.33$ ,  $t = 0.50$  and  $t = 0.85$  are illustrated in Fig. 1.

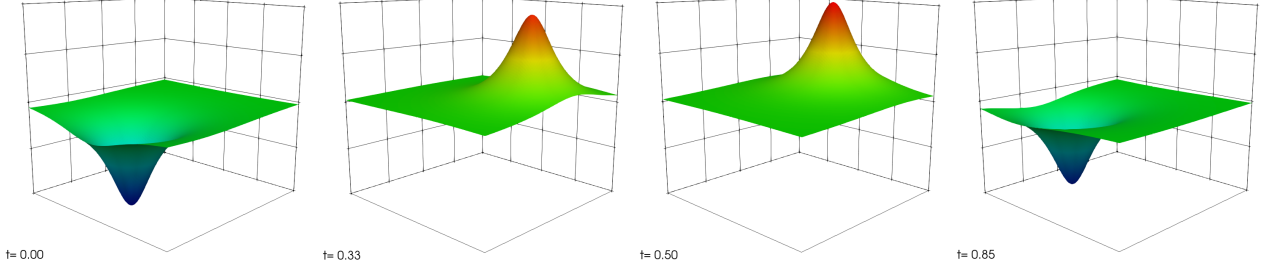


Figure 1: Solution profiles  $u_{\tau h}$  at  $t = 0$ ,  $t = 0.33$ ,  $t = 0.50$  and  $t = 0.85$  for Sec. 5.1.

The right-hand side forcing term  $g$ , the inhomogeneous Dirichlet boundary condition and the inhomogeneous initial condition are calculated from the given analytic solution (5.1) and Eqs. (1.4) (a)-(c). Our target quantity is chosen to control the global  $L^2(L^2)$ -error of  $e$ ,  $e = u - u_{\tau h}$ , in space and time, given by

$$J(\varphi) = \frac{1}{\|e\|_{(0,T) \times \Omega}} \int_I (\varphi, e) dt, \quad \text{with } \|\cdot\|_{(0,T) \times \Omega} = \left( \int_I (\cdot, \cdot) dt \right)^{\frac{1}{2}}. \quad (5.2)$$

The tuning parameters of the goal-oriented adaptive Algorithm given in Sec. 4 are chosen here in a way to balance automatically the potential misfit of the spatial and temporal errors as

$$\theta_h^{\text{top}} = 0.5 \cdot \left| \frac{\eta_h}{\eta_h + \eta_\tau} \right|, \quad \theta_h^{\text{bottom}} = 0 \quad \text{and} \quad \theta_\tau^{\text{top}} = 0.5 \cdot \left| \frac{\eta_\tau}{\eta_h + \eta_\tau} \right|.$$

$\ell$	$N$	$N_K$	$N_{\text{DoF}}^{\text{tot}}$	$\ u - u_{\tau h}^{1,1}\ $	EOC	$\ell$	$N$	$N_K$	$N_{\text{DoF}}^{\text{tot}}$	$\ u - u_{\tau h}^{2,2}\ $	EOC
1	4	4	72	8.7470e-02	—	1	5	4	375	5.3652e-02	—
2	8	16	400	2.7935e-02	1.65	2	10	16	2430	1.3714e-02	1.97
3	16	64	2592	9.0984e-03	1.62	3	20	64	17340	1.5497e-03	3.15
4	32	256	18496	3.0196e-03	1.59	4	40	256	130680	1.9911e-04	2.96
5	64	1024	139392	7.6942e-04	1.97	5	80	1024	1014000	3.5649e-05	2.48
6	128	4096	1081600	1.9290e-04	2.00	6	160	4096	7987680	5.3813e-06	2.73
7	256	16384	8520192	4.9303e-05	1.97	7	320	16384	63407040	6.8615e-07	2.97
8	512	65536	67634176	1.2490e-05	1.98						

Table 1: Global convergence for  $u_{\tau h}^{1,1}$  in a cG(1)-dG(1) and  $u_{\tau h}^{2,2}$  in a cG(2)-dG(2) primal approximation for a convection-diffusion transport problem with  $\varepsilon = 1$  and  $\delta_0 = 0$  for Sec. 5.1.  $\ell$  denotes the refinement level,  $N$  the total cells in time,  $N_K$  the cells in space on a slab,  $N_{\text{DoF}}^{\text{tot}}$  the total space-time degrees of freedom,  $\|\cdot\|$  the global  $L^2(L^2)$ -norm error and EOC the experimental order of convergence.

$\ell$	$N$	$N_K$	$N_{\text{DoF}}^{\text{tot}}$	$\ u - u_{\tau h}^{1,1}\ $	EOC	$\ell$	$N$	$N_K$	$N_{\text{DoF}}^{\text{tot}}$	$\ u - u_{\tau h}^{2,2}\ $	EOC
1	4	4	72	5.8984e-02	—	1	4	4	300	4.3801e-02	—
2	8	16	400	4.0001e-02	0.56	2	8	16	1944	1.7138e-02	1.35
3	16	64	2592	1.5534e-02	1.36	3	16	64	13872	7.9707e-03	1.10
4	32	256	18496	6.0496e-03	1.36	4	32	256	104544	3.4451e-03	1.21
5	64	1024	139392	2.2615e-03	1.42	5	64	1024	811200	1.7150e-03	1.01
6	128	4096	1081600	1.0633e-03	1.09	6	128	4096	6390144	8.6229e-04	0.99
7	256	16384	8520192	5.2811e-04	1.01	7	256	16384	50725632	4.3314e-04	0.99
8	512	65536	67634176	2.6493e-04	1.00						

Table 2: Global convergence for  $u_{\tau h}^{1,1}$  in a cG(1)-dG(1) and  $u_{\tau h}^{2,2}$  in a cG(2)-dG(2) primal approximation for a convection-dominated transport problem with  $\varepsilon = 10^{-6}$  and  $\delta_0 = 10^{-1}$  for Sec. 5.1.  $\ell$  denotes the refinement level,  $N$  the total cells in time,  $N_K$  the cells in space on a slab,  $N_{\text{DoF}}^{\text{tot}}$  the total space-time degrees of freedom,  $\|\cdot\|$  the global  $L^2(L^2)$ -norm error and EOC the experimental order of convergence.

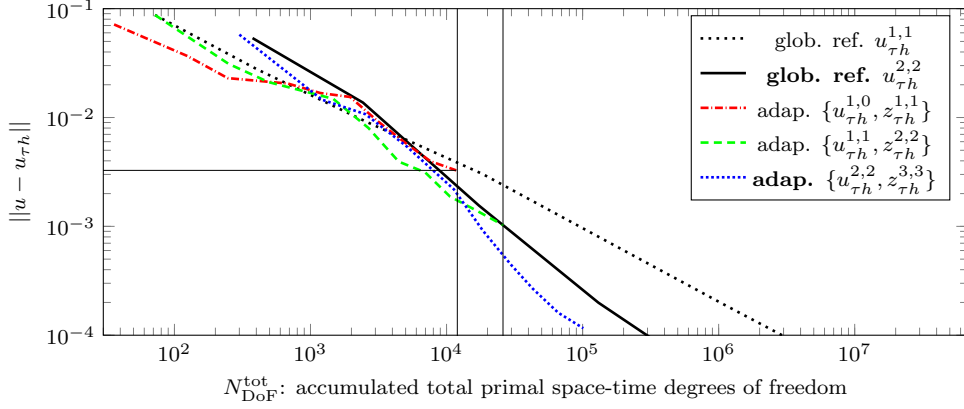


Figure 2:  $L^2(L^2)$ -error reduction in the convection-diffusion transport case with  $\varepsilon = 1$  without stabilization  $\delta_0 = 0$  for Sec. 5.1. The solution approximations are  $u_{\tau h}^{1,0}$  in cG(1)-dG(0),  $u_{\tau h}^{1,1}$  in cG(1)-dG(1),  $u_{\tau h}^{2,2}$  in cG(2)-dG(2) and the dual solution approximations are  $z_{\tau h}^{1,1}$  in cG(1)-dG(1),  $z_{\tau h}^{2,2}$  in cG(2)-dG(2),  $z_{\tau h}^{3,3}$  in cG(3)-dG(3).

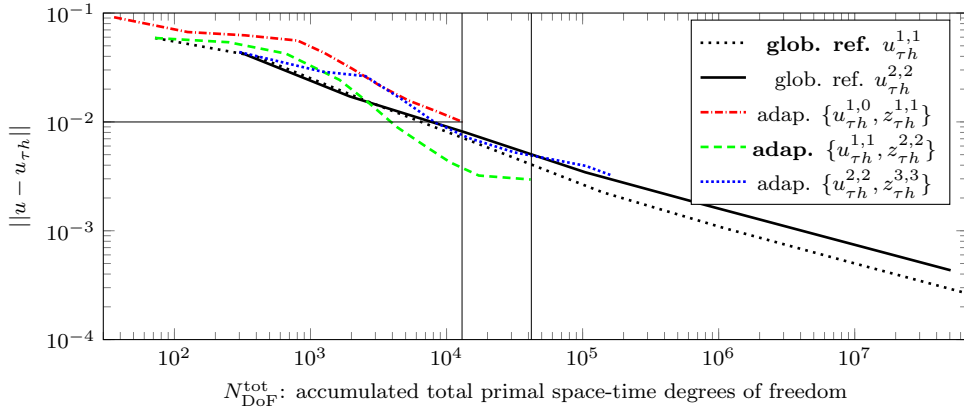


Figure 3:  $L^2(L^2)$ -error reduction in the stabilized convection-dominated transport case with  $\varepsilon = 10^{-6}$  and  $\delta_0 = 10^{-1}$  for Sec. 5.1. The solution approximations are  $u_{\tau h}^{1,0}$  in cG(1)-dG(0),  $u_{\tau h}^{1,1}$  in cG(1)-dG(1),  $u_{\tau h}^{2,2}$  in cG(2)-dG(2) and the dual solution approximations are  $z_{\tau h}^{1,1}$  in cG(1)-dG(1),  $z_{\tau h}^{2,2}$  in cG(2)-dG(2),  $z_{\tau h}^{3,3}$  in cG(3)-dG(3).

The convergence behavior, computational efficiency and stability for higher-order space-time discretizations with and without stabilization is studied in the following of this numerical experiment. Additionally, we compare global against goal-oriented space-time adaptivity. We use here a constant convection field  $\mathbf{v} = (2, 3)^\top$  for a non-stabilized convection-diffusion with  $\varepsilon = 1$  and  $\delta_0 = 0$  transport and a stabilized convection-dominated transport with  $\varepsilon = 10^{-6}$  and  $\delta_0 = 10^{-1}$  together with the constant reaction coefficient  $\alpha = 1$  and the density  $\rho = 1$ . The local SUPG stabilization coefficient is here  $\delta_K = \delta_0 \cdot h_K$  where  $h_K$  denotes the cell diameter of the spatial mesh cell  $K$ .

Initially, we study the global space-time refinement behavior for the test case with  $\varepsilon = 1$  and vanishing stabilization to show the correctness of the higher-order implementation. Therefore, the solution  $u$  is approximated with the higher-order in time method cG(1)-dG(1) and with the space-time higher-order method cG(2)-dG(2). Due to the same polynomial orders of the spatial and temporal discretizations, we expect experimental orders of convergence (EOC :=  $-\log_2(\|e\|_\ell / \|e\|_{\ell-1})$ ) of  $\text{EOC}^{1,1} \approx 2$  for the cG(1)-dG(1) method and  $\text{EOC}^{2,2} \approx 3$  for the cG(2)-dG(2) method for a global refinement convergence test. The results are given by Tab. 1 and nicely confirm our expected results for the cG(1)-dG(1) method and roughly confirm the expected results for the cG(2)-dG(2) method. The EOC of the cG(2)-dG(2) is not perfect since the initial space-time errors are not well balanced for this example.

The error reduction of the global space-time refinement results for the convection-dominated case with  $\varepsilon = 10^{-6}$  and stabilization with  $\delta_0 = 10^{-1}$  are given by Tab. 2. Both methods, that are the cG(1)-dG(1) and the cG(2)-dG(2) approximations of the primal solution  $u_{\tau h}$ , are limited in their experimental order of convergence of approximately 1. This is not a surprising result since the regularity of the convection-dominated test case is typically of low order. Therefore, we expect further the lower-order or maybe the lowest-order goal-oriented adaptivity methods to perform better than higher-order methods for the convection-dominated test case.

Secondly, we study the goal-oriented space-time adaptivity behavior. Precisely, we compare the solution

$\ell$	$N$	$N_K^{\max}$	$N_{\text{DoF}}^{\text{tot}}$	$\ e^{1,0,2,1}\ $	EOC	$\eta_h$	$\eta_\tau$	$\eta_{\tau h}$	$\mathcal{I}_{\text{eff}}$
1	4	4	36	7.1588e-02	—	5.6668e-02	1.9391e-02	7.6060e-02	1.062
2	5	16	125	3.6641e-02	0.97	7.4575e-03	2.8043e-02	3.5501e-02	0.969
3	6	28	246	2.3021e-02	0.67	5.4712e-03	3.2327e-02	3.7798e-02	1.642
4	8	76	682	2.0517e-02	0.17	2.1734e-03	2.0763e-02	2.2936e-02	1.118
5	11	88	1181	1.6786e-02	0.29	2.3597e-03	2.1533e-02	2.3892e-02	1.423
6	15	124	1959	1.5438e-02	0.12	1.4977e-03	1.4946e-02	1.6443e-02	1.065
7	21	136	3085	9.3565e-03	0.72	2.3671e-03	1.5271e-02	1.7638e-02	1.885
8	30	160	4878	5.9652e-03	0.65	2.5744e-03	1.2993e-02	1.5567e-02	2.610
9	42	172	7610	3.9673e-03	0.59	2.1052e-03	7.8182e-03	9.9234e-03	2.501
10	58	208	<b>11786</b>	<b>3.2686e-03</b>	0.28	2.4333e-03	6.3257e-03	8.7590e-03	2.680
				avg. EOC =	0.50				

Table 3:  $L^2(L^2)$ -error reduction in the convection-diffusion transport case with  $\varepsilon = 1$  without stabilization  $\delta_0 = 0$  for Sec. 5.1.  $e^{1,0,2,1}$  corresponds to the adaptive solution approximation  $u_{\tau h}^{1,0}$  in cG(1)-dG(0) and dual solution approximation  $z_{\tau h}^{2,1}$  in cG(2)-dG(1).

$\ell$	$N$	$N_K^{\max}$	$N_{\text{DoF}}^{\text{tot}}$	$\ e^{1,1,2,2}\ $	EOC	$\eta_h$	$\eta_\tau$	$\eta_{\tau h}$	$\mathcal{I}_{\text{eff}}$
1	4	4	72	8.7470e-02	—	4.7959e-02	-4.5912e-03	4.3367e-02	0.496
2	5	16	250	3.1113e-02	1.49	4.1953e-03	7.3543e-03	1.1550e-02	0.371
3	6	28	492	2.1156e-02	0.56	3.0706e-03	9.2354e-03	1.2306e-02	0.582
4	8	76	1468	1.4856e-02	0.51	2.1015e-03	6.4001e-03	8.5016e-03	0.572
5	11	124	2666	8.0165e-03	0.89	2.6080e-03	6.5137e-03	9.1217e-03	1.138
6	14	160	4456	3.9318e-03	1.03	3.1048e-03	7.1463e-03	1.0251e-02	2.607
7	18	196	<b>6960</b>	<b>3.1346e-03</b>	0.33	2.2002e-03	4.3348e-03	6.5350e-03	2.085
8	23	232	10610	1.8780e-03	0.74	5.4403e-04	1.7686e-03	2.3126e-03	1.231
9	31	280	16522	1.4014e-03	0.42	3.5661e-04	9.3709e-04	1.2937e-03	0.923
10	42	340	26252	1.0214e-03	0.46	5.1205e-05	2.8010e-04	3.3130e-04	0.324
				avg. EOC =	0.71				

Table 4:  $L^2(L^2)$ -error reduction in the convection-diffusion transport case with  $\varepsilon = 1$  without stabilization  $\delta_0 = 0$  for Sec. 5.1.  $e^{1,1,2,2}$  corresponds to the adaptive solution approximation  $u_{\tau h}^{1,1}$  in cG(1)-dG(1) and dual solution approximation  $z_{\tau h}^{2,2}$  in cG(2)-dG(2).

$\ell$	$N$	$N_K^{\max}$	$N_{\text{DoF}}^{\text{tot}}$	$\ e^{2,2,3,3}\ $	EOC	$\eta_h$	$\eta_\tau$	$\eta_{\tau h}$	$\mathcal{I}_{\text{eff}}$
1	4	4	300	5.7763e-02	—	4.1837e-03	3.6501e-03	7.8339e-03	0.136
2	5	16	1215	1.4581e-02	1.99	3.5634e-03	4.5982e-03	8.1616e-03	0.560
3	6	28	2538	1.0721e-02	0.44	5.9011e-04	4.9905e-03	5.5806e-03	0.521
4	8	76	<b>5112</b>	<b>5.4041e-03</b>	0.99	3.0895e-04	3.3977e-03	3.7067e-03	0.686
5	11	88	<b>11325</b>	<b>2.1878e-03</b>	1.30	6.4201e-04	2.7536e-03	3.3956e-03	1.552
6	15	100	18489	9.1402e-04	1.26	4.6743e-04	1.8813e-03	2.3487e-03	2.570
7	21	124	29895	4.4147e-04	1.05	3.3121e-04	1.9212e-04	5.2333e-04	1.185
8	24	184	43026	2.6759e-04	0.72	1.5650e-04	1.7675e-04	3.3325e-04	1.245
9	30	208	66270	1.6078e-04	0.73	7.4964e-05	1.5182e-04	2.2678e-04	1.410
10	40	256	101178	1.1594e-04	0.47	6.7057e-05	1.9555e-05	8.6611e-05	0.747
				avg. EOC =	0.99				

Table 5:  $L^2(L^2)$ -error reduction in the convection-diffusion transport case with  $\varepsilon = 1$  without stabilization  $\delta_0 = 0$  for Sec. 5.1.  $e^{2,2,3,3}$  corresponds to the adaptive solution approximation  $u_{\tau h}^{2,2}$  in cG(2)-dG(2) and dual solution approximation  $z_{\tau h}^{3,3}$  in cG(3)-dG(3).

and dual solution approximation pairings  $\{u_{\tau h}, z_{\tau h}\}$ : cG(1)-dG(0)/cG(2)-dG(1), cG(1)-dG(1)/cG(2)-dG(2) and cG(2)-dG(2)/cG(3)-dG(3). The lowest-order results can be compared with the results of our preceding published work [10], while remarking that a cG(1)-dG(0)/cG(2)-cG(1) discretization was used there combined with a different choice for the tuning parameters. The results are given by Fig. 2 and by Tab. 3-5. Here, the adaptive method of highest order, i.e. the approximation by cG(2)-dG(2)/cG(3)-dG(3), outperforms all other methods.

Finally, we study the goal-oriented space-time adaptivity behavior for the convection-dominated case with  $\varepsilon = 10^{-6}$ . Precisely, we compare the solution and dual solution approximation pairings  $\{u_{\tau h}, z_{\tau h}\}$ : cG(1)-dG(0)/cG(2)-dG(1), cG(1)-dG(1)/cG(2)-dG(2) and cG(2)-dG(2)/cG(3)-dG(3). The lowest-order results can be compared with the results of our preceding published work [10], while remarking that a cG(1)-dG(0)/cG(2)-cG(1) discretization was used there combined with a different choice for the tuning parameters. The results are given by Fig. 3 and by Tab. 6-8. Here, the low order method, but not lowest order, i.e. the approximation by cG(1)-dG(1)/cG(2)-dG(2), outperforms all other methods.

$\ell$	$N$	$N_K^{\max}$	$N_{\text{DoF}}^{\text{tot}}$	$\ e^{1,0,2,1}\ $	EOC	$\eta_h$	$\eta_\tau$	$\eta_{\tau h}$	$\mathcal{I}_{\text{eff}}$
1	4	4	36	9.1527e-02	—	3.6697e-02	1.5147e-02	5.1844e-02	0.566
2	5	16	125	6.6916e-02	0.45	6.4515e-03	-6.0024e-04	5.8513e-03	0.087
3	6	52	330	6.2426e-02	0.10	2.6882e-03	5.9916e-03	8.6798e-03	0.139
4	8	88	804	5.5849e-02	0.16	2.1670e-03	6.6884e-03	8.8554e-03	0.159
5	11	100	1265	4.3011e-02	0.38	3.2302e-03	1.1793e-02	1.5023e-02	0.349
6	15	124	2037	3.0684e-02	0.49	2.3297e-03	1.3276e-02	1.5605e-02	0.509
7	21	160	3283	2.1294e-02	0.53	1.8278e-03	1.1939e-02	1.3767e-02	0.647
8	30	184	5262	1.5710e-02	0.44	2.7619e-03	1.0873e-02	1.3635e-02	0.868
9	41	220	8357	1.2567e-02	0.32	3.3126e-03	7.9147e-03	1.1227e-02	0.893
10	55	280	<b>13121</b>	<b>9.9855e-03</b>	0.33	5.5998e-03	6.5796e-03	1.2179e-02	1.220
				avg. EOC =	0.36				

Table 6:  $L^2(L^2)$ -error reduction in the stabilized convection-dominated transport case with  $\varepsilon = 10^{-6}$  and  $\delta_0 = 10^{-1}$  for Sec. 5.1.  $e^{1,0,2,1}$  corresponds to the adaptive solution approximation  $u_{\tau h}^{1,0}$  in cG(1)-dG(0) and dual solution approximation  $z_{\tau h}^{2,1}$  in cG(2)-dG(1).

$\ell$	$N$	$N_K^{\max}$	$N_{\text{DoF}}^{\text{tot}}$	$\ e^{1,1,2,2}\ $	EOC	$\eta_h$	$\eta_\tau$	$\eta_{\tau h}$	$\mathcal{I}_{\text{eff}}$
1	4	4	72	5.8984e-02	—	2.6394e-02	1.3546e-03	2.7749e-02	0.470
2	5	16	250	5.3935e-02	0.13	-1.4730e-02	3.8407e-03	-1.0889e-02	0.202
3	6	52	660	4.2387e-02	0.35	-5.4370e-04	4.7724e-03	4.2287e-03	0.100
4	9	76	1634	2.4328e-02	0.80	1.2300e-03	4.5411e-03	5.7711e-03	0.237
5	12	124	2668	1.5031e-02	0.69	7.6984e-03	4.4589e-03	1.2157e-02	0.809
6	14	172	<b>4316</b>	<b>8.9709e-03</b>	0.74	2.7195e-03	5.1674e-03	7.8869e-03	0.879
7	18	208	7032	5.9470e-03	0.59	3.2797e-03	3.1406e-03	6.4202e-03	1.080
8	22	268	10668	4.2404e-03	0.49	-1.1081e-04	1.7962e-03	1.6854e-03	0.397
9	33	292	17270	3.2138e-03	0.40	-1.8817e-03	7.9462e-04	-1.0871e-03	0.338
10	45	568	41550	2.9555e-03	0.12	-8.4016e-03	3.2177e-04	-8.0798e-03	2.734
				avg. EOC =	0.48				

Table 7:  $L^2(L^2)$ -error reduction in the stabilized convection-dominated transport case with  $\varepsilon = 10^{-6}$  and  $\delta_0 = 10^{-1}$  for Sec. 5.1.  $e^{1,1,2,2}$  corresponds to the adaptive solution approximation  $u_{\tau h}^{1,1}$  in cG(1)-dG(1) and dual solution approximation  $z_{\tau h}^{2,2}$  in cG(2)-dG(2).

$\ell$	$N$	$N_K^{\max}$	$N_{\text{DoF}}^{\text{tot}}$	$\ e^{2,2,3,3}\ $	EOC	$\eta_h$	$\eta_\tau$	$\eta_{\tau h}$	$\mathcal{I}_{\text{eff}}$
1	4	4	300	4.3801e-02	—	-2.6854e-03	1.0697e-03	-1.6156e-03	0.037
2	5	16	1215	2.8964e-02	0.60	2.2071e-03	2.3582e-03	4.5653e-03	0.158
3	6	28	2538	2.6314e-02	0.14	1.0415e-03	2.0664e-03	3.1078e-03	0.118
4	7	76	4719	1.6058e-02	0.71	6.6330e-04	2.2853e-03	2.9486e-03	0.184
5	9	88	<b>8175</b>	<b>9.9382e-03</b>	0.69	4.8613e-04	1.9507e-03	2.4369e-03	0.245
6	12	124	14442	7.1355e-03	0.48	-5.9480e-04	1.0807e-03	4.8594e-04	0.068
7	18	244	31548	5.2461e-03	0.44	-1.7721e-03	6.0417e-04	-1.1680e-03	0.223
8	22	376	66042	4.4188e-03	0.25	-1.1307e-03	1.0326e-04	-1.0275e-03	0.233
9	23	556	105825	3.9399e-03	0.17	-1.3787e-03	-8.2448e-05	-1.4611e-03	0.371
10	24	868	164886	3.2102e-03	0.30	-1.0300e-03	-1.4457e-04	-1.1746e-03	0.366
				avg. EOC =	0.42				

Table 8:  $L^2(L^2)$ -error reduction in the stabilized convection-dominated transport case with  $\varepsilon = 10^{-6}$  and  $\delta_0 = 10^{-1}$  for Sec. 5.1.  $e^{2,2,3,3}$  corresponds to the adaptive solution approximation  $u_{\tau h}^{2,2}$  in cG(2)-dG(2) and dual solution approximation  $z_{\tau h}^{3,3}$  in cG(3)-dG(3).

## 5.2. Example 2 (Transport in a Channel)

In this example we simulate a convection-dominated transport with goal-oriented adaptivity of a species through a channel with a constraint. The domain and its boundary colorization are presented by Fig. 4. Precisely, the spatial domain is composed of two unit squares and a constraint in the middle which restricts the channel height by a factor of 5. Precisely,  $\Omega = (-1, 0) \times (-0.5, 0.5) \cup (0, 1) \times (-0.1, 0.1) \cup (1, 2) \times (-0.5, 0.5)$  with an initial cell diameter of  $h = \sqrt{2 \cdot 0.025^2}$ . The time domain is set to  $I = (0, 2.5)$  with an initial  $\tau = 0.1$  for the initialization of the slabs for the first loop  $\ell = 1$ . We approximate the primal solution  $u_{\tau h}^{1,1}$  with the cG(1)-dG(1) method and the dual solution  $z_{\tau h}^{2,2}$  with the cG(2)-dG(2) method. The target quantity is

$$J(\varphi) = \frac{1}{\|u_{\tau h}\|_{(0,T) \times \Omega}} \int_I (\varphi, u_{\tau h}) \, dt.$$



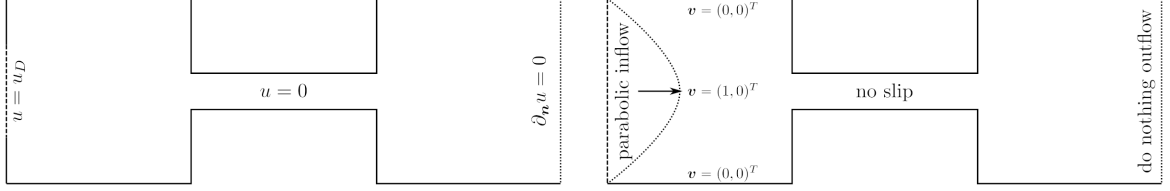


Figure 4: Boundary colorization for the convection-diffusion problem (left) and the coupled Stokes problem (right) for Sec. 5.2.

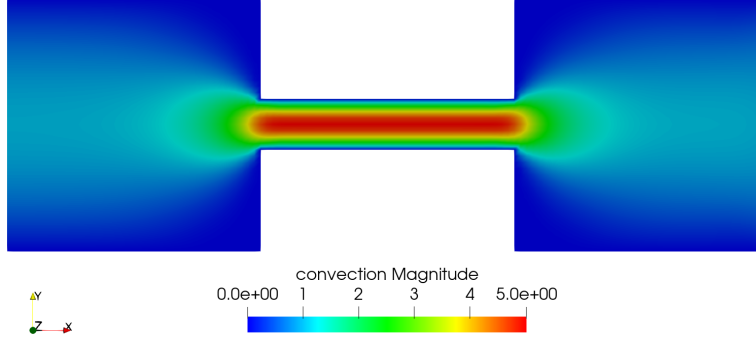


Figure 5: Convection  $v_h$  solution of the Stokes problem on a sufficiently globally refined mesh with  $Q_2$ - $Q_1$  finite elements for Sec. 5.2. On the left boundary a parabolic inflow profile in the positive x-direction with unit magnitude is prescribed for the convection  $v$ .

The transport of the species, which enters the domain on the left with an inhomogeneous and time-dependent Dirichlet boundary condition and leaves the domain on the right through a homogeneous Neumann boundary condition, is driven by the convection with magnitudes between 0 and 5 as displayed in Fig. 5. The diffusion coefficient has the constant and small value of  $\varepsilon = 10^{-4}$ , the reaction coefficient  $\alpha = 0$  is vanishing and the density has the value  $\rho = 1$ . The local SUPG stabilization coefficient is here set to  $\delta_K = \delta_0 \cdot h_K$ ,  $\delta_0 = 0$ , i.e. a vanishing stabilization here. The initial value function  $u_0 = 0$  as well as the forcing term  $g = 0$  are homogeneous. The Dirichlet boundary function value is homogeneous on  $\Gamma_D$  except for the line  $(-1, -1) \times (-0.25, 0.25)$  where the value

$$u(y, t) = 16 \cdot (0.25 - y) \cdot (y + 0.25) \cdot \min\{100t, 0.1\}$$

is prescribed on the solution. The viscosity is set to  $\tilde{\nu} = 1$ . The tuning parameters of the goal-oriented adaptive Algorithm given in Sec. 4 are chosen here in a way to balance automatically the potential misfit of the spatial and temporal errors as  $\theta_h^{\text{bottom}} = 0$ ,

$$\theta_h^{\text{top}} = \frac{1}{2} \cdot \min \left\{ \left| \frac{\eta_h}{\eta_h + \eta_\tau} \right|, 1 \right\} \quad \text{and} \quad \theta_\tau^{\text{top}} = \frac{1}{2} \cdot \min \left\{ \left| \frac{\eta_\tau}{\eta_h + \eta_\tau} \right|, 1 \right\}.$$

$\ell$	$N$	$N_K^{\text{tot}}$	$N_K^{\text{max}}$	$\ u_{\tau h}^{1,1}\ $
1	25	88000	3520	0.0845694
2	26	108380	5008	0.0843620
3	27	153324	8464	0.0844429
4	28	203524	10792	0.0845339
5	29	298952	17680	0.0846325
6	30	459696	25996	0.0847412
7	31	649852	38212	0.0848211
8	32	1058456	68344	0.0848755
9	41	1881548	100744	0.0849878

Table 9: Goal-oriented temporal and spatial refinements for Sec. 5.2.  $\ell$  denotes the refinement level loop,  $N$  the accumulated total cells in time,  $N_K^{\text{tot}}$  the accumulated total cells in space,  $N_K^{\text{max}}$  the maximal number of cells on a slab and  $\|u_{\tau h}^{1,1}\|$  the value of the goal-functional.

The solution profiles and corresponding adaptive meshes of the primal solution  $u_{\tau h}^{1,1}$  of the loop  $\ell = 5$  for  $t = 0.82$ ,  $t = 1.32$  and  $t = 2.28$  are given by Fig. 6. In Fig. 7 we present a comparative study of the solution profile and corresponding meshes for  $t = 1.21$  over the adaptivity loops. For  $\ell = 1, 2, 3$  obvious spurious oscillations in the left square are existing, which are captured and resolved by the goal-oriented adaptivity by taking spatial mesh refinements next to the right boundary of the left square. For  $\ell > 3$  the spatial refinements

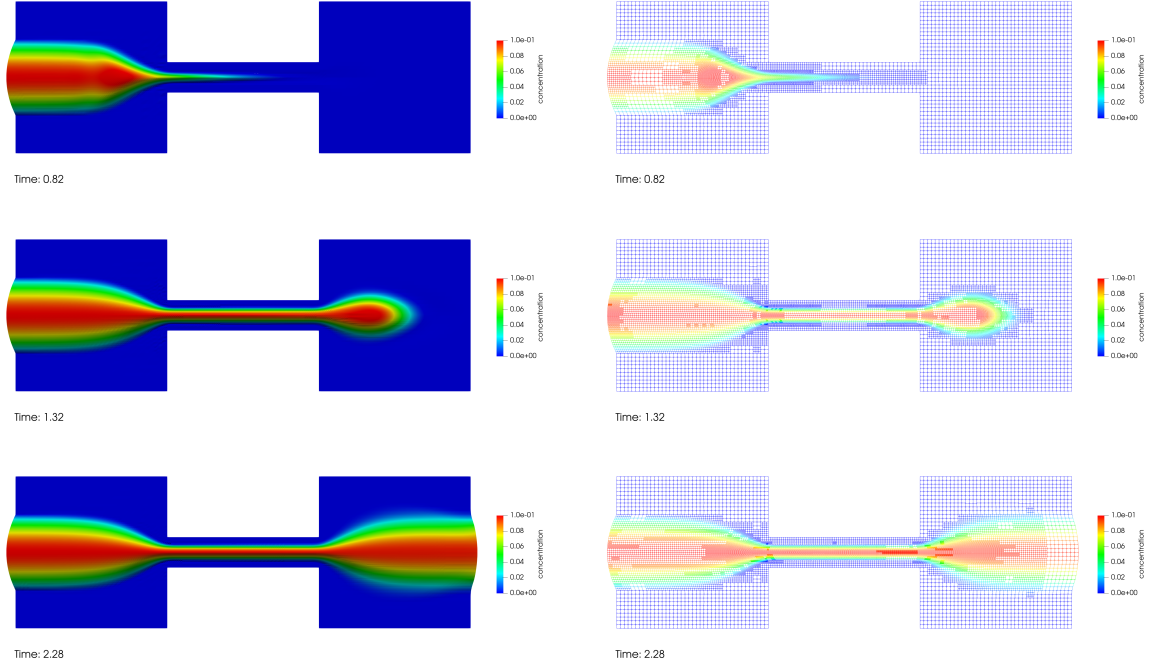


Figure 6: Solution profiles and corresponding meshes of loop  $\ell = 5$  for Sec. 5.2.

capture especially the solution profile fronts with strong gradients with a focus on the high-convective middle of the spatial domain. The refinement in time is very little compared to the refinement in space here as given by Tab. 9, due to the intelligent choice of the tuning parameters for the spatial and temporal refinements.

## 6. Summary

In this work we presented an space-time adaptive solution algorithm for SUPG stabilized finite element approximations of a convection-dominated transport problem that is coupled with a flow problem. The convection-dominance puts further facets of complexity and sensitivity on the a-posteriori error control, but also illustrates the efficiency and potential of automatic mesh adaptation. The underlying approach is based on the Dual Weighted Residual method for goal-oriented error control. A splitting of the discretization errors in space and time is used for the transport problem which is then used for the respective mesh adaptation process in the form of underlying error indicators  $\eta_\tau$  and  $\eta_h$ , respectively. A discontinuous Galerkin method dG( $r$ ) with an arbitrary polynomial degree  $r \geq 0$  is applied for the discretization in time of the transport problem. We use a higher-order finite element approximation in space and time in order to compute the dual solution. In numerical experiments we could prove that spurious oscillations that typically arise in numerical approximations of convection-dominated problems could be reduced significantly. Effectivity indices close to one were obtained for small diffusion coefficients corresponding to high Péclet numbers. Moreover, the potential of the approach was illustrated for a problem of practical interest. Along with the underlying software platform, even more sophisticated techniques and settings including multirate approximations, varying meshes for flow and transport or coupling with time-dependent flow problems become feasible.

## Acknowledgements

U. Köcher was partially supported by the Oden Institute for Computational Engineering and Sciences, University of Texas at Austin, Texas, USA as long-term guest visitor of M.F. Wheeler for the implementation of the used space-time-slab finite element handler.

## References

- [1] Almani, T., Kumar, K., Dogru, A., Singh, G., Wheeler, M.F.: Convergence analysis of multirate fixed-stress split iterative schemes for coupling flow with geomechanics. *Comput. Meth. Appl. Mech. Engrg.* **311**, 180–207 (2016)

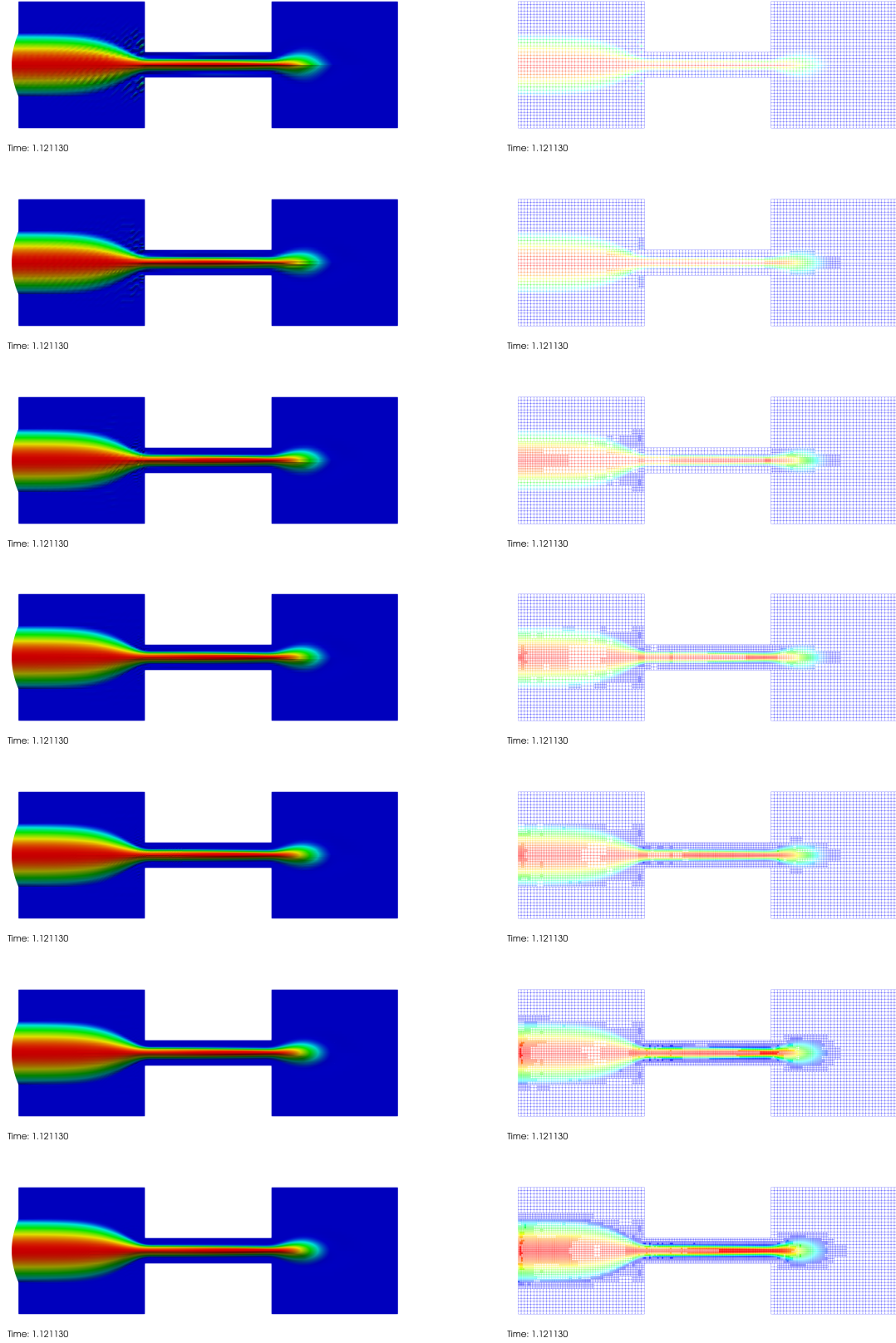


Figure 7: Capturing of spurious oscillations with goal-oriented adaptivity illustrated by comparative solution profiles and corresponding meshes of the loops  $\ell = 1 - 7$  for Sec. 5.2.

- [2] Arndt, D., Bangerth, W., Clevenger, T., Davydov, D., Fehling, M., Garcia-Sanchez, D., Harper, G., Heister, T., Heltai, L., Kronbichler, M., Maguire Kynch, R., Maier, M., Pelteret, J.P., Turcksin, B., Wells, D.: The `deal.II` Library, Version 9.1, *J. Numer. Math.* (2019). doi:10.1515/jnma-2019-0064, pp. 1–14.
- [3] Bangerth, W., Geiger, M., Rannacher, R.: Adaptive Galerkin finite element methods for the wave equation. *Comput. Meth. Appl. Math.* **10**, 3–48 (2010)
- [4] Bangerth, W., Rannacher, R.: Adaptive finite element methods for differential equations. Birkhäuser, Basel (2003)
- [5] Becker, R., Rannacher, R.: An optimal control approach to a posteriori error estimation in finite element methods. In: Iserles, A. (ed.) *Acta Numer.*, vol. 10, pp. 1–102. Cambridge University Press (2001)
- [6] Besier, M., Rannacher, R.: Goal-oriented space-time adaptivity in the finite element Galerkin method for the computation of nonstationary incompressible flow. *Int. J. Num. Methods Fluids* **70**(9), 1139–1166 (2012)
- [7] Braack, M., Ern, A.: A posteriori control of modeling errors and discretization errors. *Multiscale Model. Simul.* **1**, 221–238 (2003)
- [8] Brooks, A. N., Hughes, T. J. R.: Streamline upwind/Petrov-Galerkin formulations for convection dominated flows with particular emphasis on the incompressible Navier-Stokes equations. *Comput. Methods Appl. Mech. Engrg.* **32**(1-3), 199–259 (1982)
- [9] Bruchhäuser, M. P., Schwegler, K., Bause, M.: Numerical study of goal-oriented error control for stabilized finite element methods. In: Apel, T. et al. (eds.) *Advanced Finite Element Methods with Applications. FEM 2017, Lecture Notes in Computational Science and Engineering* **128**, Springer, Cham, 2019, 85–106 doi:10.1007/978-3-030-14244-5\_5, (2019)
- [10] Bruchhäuser, M. P., Schwegler, K., Bause, M.: Dual weighted residual based error control for nonstationary convection-dominated equations: potential or ballast? In: Barrenechea G. et al. (eds.), *BAIL 2018 – Boundary and Interior Layers, in press*, *Lecture Notes in Computational Science and Engineering* **126**, Springer, Cham, 2019, 13 pp. arXiv:1812.06810
- [11] Carey, G. F., Oden, J. T.: *Finite Elements, Computational Aspects, Vol. III (The Texas finite element series)*. Prentice-Hall, Englewood Cliffs, New Jersey (1984)
- [12] Endtmayer, B., Wick, T.: A partition-of-unity dual-weighted residual approach for multiple objective goal functional error estimation applied to elliptic problems. *Comput. Methods Appl. Math.* **17**, 575–599 (2017)
- [13] Endtmayer, B., Langer, U., Wick, T.: Two-side a posteriori error estimates for the DWR method, *SIAM J. Sci. Comput.*, in press (2019); arXiv:1811.07586
- [14] Ge, Z., Ma, M.: Multirate iterative scheme based on multiphysics discontinuous Galerkin method for a poroelasticity model. *Appl. Numer. Math.* **128**, 125–138 (2018)
- [15] Ge, Z., Ma, M.: Multiphysics discontinuous Galerkin method for a poroelasticity model. *Appl. Math. Comput.* **301**, 78–94 (2017)
- [16] Gupta, S., Wohlmuth, B., Helmig, R.: Multirate time stepping schemes for hydro-geomechanical model for subsurface methane hydrate reservoirs. *Adv Water Res.* **91**, 78–87 (2016)
- [17] Hughes, T. J. R., Brooks, A. N.: A multidimensional upwind scheme with no crosswind diffusion. In: Hughes, T. J. R. (eds.) *Finite Element Methods for Convection Dominated Flows, AMD*, vol. 34, pp. 19–35. Amer. Soc. Mech. Engrs. (ASME) (1979)
- [18] John, V., Novo, J.: Error analysis of the SUPG finite element discretization of evolutionary convection-diffusion-reaction equations. *SIAM J. Numer. Anal.* **49**(3), 1149–1176 (2011)
- [19] John, V., Knobloch, P., Novo, J.: Finite elements for scalar convection-dominated equations and incompressible flow problems: a never ending story? *Comput. Vis. Sci.*, doi:10.1007/s00791-018-0290-5, 1–17 (2018)
- [20] John, V., Schmeyer, E.: Finite element methods for time-dependent convection-diffusion-reaction equations with small diffusion. *Comput. Methods Appl. Mech. Engrg.* **198**, 173–181 (2009)

- [21] Kanschat, G., Riviere, B.: A finite element method with strong mass conservation for Biot’s linear consolidation model. *J. Sci. Comp.* **77**, 1762–1779 (2018)
- [22] Köcher, U., Bruchhäuser, M. P., Bause, M.: Efficient and scalable data structures and algorithms for goal-oriented adaptivity of space-time FEM codes. *SoftwareX* **10**:1-6, 100239, doi:10.1016/j.softx.2019.100239, in press (2019)
- [23] Larson, M.G., Malquist, A.: Goal oriented adaptivity for coupled flow and transport with applications in oil reservoir simulations. *Comput. Methods Appl. Mech. Engrg.* **196**, 3546–3561 (2007)
- [24] Li, S.Y.: A study of two modes of locking in poroelasticity. *SIAM J. Numer. Anal.* **55**, 1915–1936 (2017)
- [25] Mikelić, A., Wheeler, M.F.: Convergence of iterative coupling for coupled flow and geomechanics. *Comput. Geosci.* **17**, 479–496 (2013)
- [26] Rannacher, R., Vihharev, J.: Adaptive finite element analysis of nonlinear problems: balancing of discretization and iteration errors. *J. Numer. Math.* **21**, 23–61 (2013)
- [27] Richter, T.: *Fluid–Structure Interactions: Models, Analysis and Finite Elements*, Lecture Notes in Computational Science and Engineering, vol. 118. Springer, Berlin (2017)
- [28] Roos, H.-G., Stynes, M., Tobiska, L.: *Robust Numerical Methods for Singularly Perturbed Differential Equations*. Springer, Berlin (2008)
- [29] Sauer-Budge, A.M., Bonet, J., Huerta, A., Peraire, J.: Computing bounds for linear functionals of exact weak solutions to Poissons equation. *SIAM J. Numer. Anal.* **42**(4), 1610–1630 (2004)
- [30] Schmich, M., Vexler, B.: Adaptivity with dynamic meshes for space-time finite element discretizations of parabolic equations. *SIAM J. Sci. Comput.* **30**, 369–393 (2008)
- [31] Showalter, R.: Diffusion in poro-elastic media. *J. Math. Anal. Appl.* **251**, 310–340 (2000)
- [32] Wick, T.: Goal functional evaluations for phase-field fracture using PU-based DWR mesh adaptivity. *Comput. Mech.* **57**, 1017–1035 (2016)